Investigation of Coke Formation in Steam Cracking of Atmospheric Gasoil

Sorood Zahedi Abghari

* Modeling and process control Department, Process Engineering Development Division, Research Institute of Petroleum Industry (RIPI)

Email address: zahedis@ripi.ir

Abstract

To investigate the characteristics of atmospheric gasoil as a suitable feed stock of steam cracker processes, several experiments were designed and carried out in a pilot plant. The operating conditions of the designed experiments were coil outlet temperature (COT), feed flow rate and steam ratio (STR). A group of these experiments were conducted to determine the coke formation rate. Central composite design methodology was utilized to set the experiments and analysis the results. Some statistical tests were used for confirmation of the accuracy, consistency and reproducibility of experimental results. Moreover, statistical model was utilized for investigation of the coke formation rate. To determine the yield distribution of main products a reaction network consists of 21 reactions together with the related kinetic reactions rates were developed. Based on the developed models and utilizing suitable optimization algorithm, the best operating conditions were determined. The results declared that at the 883.9°C as coil outlet temperature,0.62 as steam ratio and residence time equal to 0.3 sec the optima levels were obtained in which the yield of ethylene, propylene and butadienes were respectively equal to 28.73%,12.33% and 4.02%.

Keywords

Steam Cracking; Atmospheric Gasoil; Olefins; Modeling; Optimization

Introduction

Olefins are widely used as basic species in production of polymeric material in petrochemical complexes. Ethylene as one of the main light olefins is widely produced in the world. It's globally production was 107 million tones in 2005 and 109 million tones in 2006.By 2010 ethylene was produced by at least 117 companies in 55 countries. To meet the ever increasing demand for ethylene, sharp increases in production facilities are added globally, particularly in the Persian Gulf countries and in China [1].Over 80% of ethylene is used to produce ethylene oxide, ethylene dichloride and different polyethylenes. Between products, low density and linear poly ethylene are widely demanded products [2]. Propylene as the other light olefins has been mass produced since sixty years ago. It is used to produce propylene oxide, polypropylenes, propanol and the other related chemicals [3]. Steam cracking process is the main commercial unit for mass production of these olefin species in petrochemical complexes. In this process, gas or liquid hydrocarbons are heated to temperature in the range of 770°C to 870°C .In this range of temperature, the radical reactions are accelerated. These kinds of reactions convert heavy hydrocarbons to lighter ones and the saturated species are converted to unsaturated. The complex mixture is yielded from the proposed reaction network which contains propylene and ethylene. The produced mixture is sent to some separation equipments to separate and purify the valuable produced species.

Coke as one of side product of the process is produced in the secondary steam cracking reactions and settled down in the reactor and TLE (Transfer Line Exchanger). This reduces the heat transfer rate, increases the pressure drop and the possibility of formation of hot spots. The amount of formed coke depends on the feed stock characteristics, operating conditions and the alloy used in the reactor pipe. The amount of contaminated coke on the inner wall of the pipe is increased by passing the time. To lower the effects of coke on the efficiency of the process the reactor temperature are increased. This also increases the coke formation rate and at last it causes to shut down the reactor furnace to clean up [4].

Coke formation is a complex phenomenon which follows from four different mechanisms:

1. Catalytic coke formation
2. Pyrolytic coke formation
3. Condensation mechanism of coke formation
4. Transformation of coke to down streams

In the first step, the heterogeneous reactions are carried out on the metal surface as heterogeneous catalyst of reactor pipes and consequently the filamentous coke is formed [5]. This has the highest rate in comparison with the other coke formation mechanisms while the operating temperature is low and in the range of 500°C to 600°C and the process is at the starting levels. In the pyrolytic coke formation mechanism which is also known as radical coke mechanism, the coke precursors joint to the coke surface and grow the coke [6]. In this mechanism several species as acetylenes, olefins, aromatics and paraffins incorporate in different reactions to form this kind of coke. The highest reaction rates belong to the reactions in which the acetylene is involved and the lowest is for the reactions with paraffins as reactants. The produced coke has amorphous structure [7]. The other steps of coke formation as condensation mechanism and coke transformation are highlighted at the end of reactor while the operating temperature is decreased.

Due to vitality of coke formation in thermal cracking processes, several researchers focused on this subject. The effect of operating conditions as residence time, temperature and partial pressure are investigated by Kunzru and Kumar [8]. Sundram and Froment [9] conducted other research to develop a rigorous model to predict the coke formation. In the proposed model the propylene used as the major coke precursor. The effects of alloys and materials used in the reactor pipes and the coke precursors in gas thermal cracking are studied by Zou et al [10]. Marin & Wauters [11], developed a more precise model to investigate coke formation rate. The proposed reaction network had 14000 reactions and 2400 species for ethane thermal cracking.

To inhibit or to lessen the coke formation, several researchers focused on the coke inhibitors [12-15]. The effect of DMDS as one of the coke inhibitors are studied by Dhuyvetter et al [12].Moreover, the effect of H_2PtCl_6 as coke inhibitor is studied by Chan et al [13].The power of Thiophene and benzothiozol to inhibit the formation of coke in thermal cracking of atmospheric gasoil is clarified in the Shubo et al research [14]. Also, the effect of a mixture of components contained Zn, Si and Sulphurous compounds is investigated by Brown et al [15].

In this research, by carrying out several experiments designed and analyzed based on central composite design methodology the effects of different operating variables on coke formation are estimated. Also, a statistical and a rigorous kinetic model are developed to predict the coke formation rate and the yield of main primary and secondary products. Then the optimization is carried out to determine the optimal point and the best reactor temperature profile.

Experimental Section

Feed Stock Specification

The feed stock of steam cracking pilot plant is an atmospheric gasoil with a boiling range of 218ºC to 387ºC, with a density of 0.845 gr/cm3. The total sulfur of the feed stock is approximated around 0.75 wt%. The main specifications of this oil cut are listed in Table1.

TABLE 1 THE MAIN PROPERTIES OF THE ATMOSPHERIC GASOIL

Specification	**Gas-oil**
Nitrogen, Total wt%	<0.5
Hydrogen, Total wt%	13.8
Carbon, Total wt%	85.6
Aromatic Content, vol%	14
Olefin content, vol%	Trace<0.3
Saturate Content, vol%	86
Distillation (D86):	°C
IBP at 760 mm Hg	218
5%Vol. Recovery	257
10%Vol. Recovery	266
FBP at 760 mm Hg	387

Pilot Plant Setup:

The selected experiments were performed in a steam cracking pilot setup that was designed and assembled for steam cracking of the hydrocarbon feed stocks in the range from ethane to vacuum gasoils. The hydrocarbon feed stock and the diluted water are first preheated to the hydrocarbon cracking temperature(approximately 550ºC) then mixed together and fed to the reactor in which the main cracking reactions are take place and the reactant mixture are heated up to 860ºC. The reactor effluent would be immediately quenched by cooling water in a double pipe heat exchanger. In order to separate the condensate from the gaseous product stream, the

exchanger outlet stream is sent to a flash drum. Then, the gas phase enters a series of condensers, passing through a filter in the final stage.

Experiments

Central composite design methodology was applied to design the experiments. This is used with three design factor, namely, the hydrocarbon feed flow rate(X1), the steam ratio(X2) and coil outlet temperature(X3). The coded level and the natural values of the mentioned variable are clarified in Table 2.

The number of trials was based on the number of design factors and was equal to 19 experiments (15 combinations with four replications).The results of experiments and the design matrix are shown in table3.

As introduced in Table3, the maximum coke formation rate is obtained while the coil outlet temperature, steam ratio and feed flow rate are respectively equal to 1,-1 and -1 in coded level, while minimum coke formation rate is obtained for coil outlet temperature, steam ratio and feed flow rate equal to -1,1 and 1 in coded levels.

TABLE 2 CODED AND NATURAL LEVELS OF THE DESIGN FACTORS.

Design Factors	-1.6818	-1	0	1	1.6818
Feed Flow rate	0.98	2	3.5	5	6.00
Steam ratio	0.4636	0.6	0.8	1	1.13636
Coil Outlet temperature	716	750	800	850	884

TABLE 3 DESIGN MATRIX AND RESULTS OF THE CENTRAL COMPOSITE DESIGN

No	1	2	3	4	5	6	7	8	9	10	11	12	13	14	15	16	17	18	19
Feed Flow rate	-1	-1	-1	-1	1	1	1	1	-1.68	1.68	0	0	0	0	0	0	0	-1	-1
Steam ratio	-1	-1	1	1	-1	-1	1	1	0	0	-1.68	1.68	0	0	0	0	0	1	1
Coil Outlet temperature	-1	1	-1	1	-1	1	-1	1	0	0	0	0	-1.68	1.68	0	0	0	1	1
Rate of Coke (gr/cm².sec) 10^7	1.67	34.1	0.66	20.9	0.16	18.2	0.03	3.9	12.3	0.51	11.53	0.65	0.06	32.4	1.6	2.35	2.4	24.6	25.6

Modeling Section

Two different models as statistical and rigorous kinetic model are used to investigate the coke formation rate and product yield distribution. The following full quadratic model was used to develop the statistical model. It is obtained by a multiple regression technique for three factors.

$$Y_i=\alpha+\beta_1X_1+\beta_2X_2+\beta_3X_3+\beta_{11}X_1^2+\beta_{22}X_2^2+\beta_{33}X_3^2+\beta_{12}X_1X_2+\beta_{13}X_1X_3+\beta_{23}X_2X_3 \quad (1)$$

In table 4, the significance of different factors and their interactions, the related coefficient, the ANOVA results for lack-of-fit and the result of R-squared tests have been shown.

This table introduces the significant and insignificant parameters by declaring the p-value. The vital value for "p" is 0.05. The values less than this border point introduce the significant parameters. The insignificant parameters are discarded with a confidence level of 95% while their p-value are higher than 0.05.The p-value of lack of fit is used to determine whether or not the constructed model was appropriate to describe the observed data.

To investigate the yield distribution of main products a molecular reaction network is introduced. Based on the introduced reaction network, reaction mixture is divided into two different sections as primary pyrolysis and dissociation sections. The primary reactions are the only chemical phenomena happened in the first section. However, in the second section the decomposition and polymerization reactions occurred and the primary and secondary reaction product accompanied as the reactants. Pyrolysis-oil which contains several aromatic species is one of the second section reactions products.

TABLE 4TEST OF SIGNIFICANCE OF FACTORS AND INTERACTIONS FOR STATISTICAL MODEL OF COKE FORMATION, R-SQUARED AND LACK-OF-FIT

Factor or Interaction	Rate of Coke formation * 10^7 (gr/cm2.sec)		
	Coefficient	T	p-value
Constant	968.57	7.231	0
X_1	38.013	5.41	0
X_2	193.05	3.796	0.004
X_3	-2.92	-8.838	0
X_1*X_1	0.47689	2.093	0.066
X_2*X_2	16.388	2.438	0.037
X_3*X_3	0.002193	10.442	0
X_1*X_2	-0.6494	-0.294	0.775
X_1*X_3	-0.05453	-6.517	0
X_2*X_3	-0.28708	-4.795	0.001
R-Squared	99.10%		
Value of lack of fit	0.073		

To demonstrate the primary reactions, the following pseudo reaction is introduced [16]:

$$Feedstock \xrightarrow{r_1} aH_2 + bCH_4 + cC_2H_4 + dC_2H_6 + eC_3H_8 + fC_3H_6 + gC_4H_8 + hC_4H_6 + iC_2H_2 + jC_4H_{10} \quad (2)$$

Second part of reactions network contain several reactions to decompose or combine the ten products yielded from reaction demonstrated in equation(2).Table(5) clarifies reactions happens in this section. In this table, EB and B refer to Ethyl benzene and benzene respectively. To consider, other aromatic species a pseudo species "C6.5 H7"is defined. Also "L" refers to pseudo component with 7.5 carbons.

TABLE 5. THE REACTIONS OF SECONDARY SECTIONS IN REACTION NETWORK

Reaction No	Reaction	$A\left(\frac{1}{S}\right)$	$E\left(\frac{kJ}{mol}\right)$
1	$C_2H_6 \leftrightarrow C_2H_4 + H_2$	$7.54x10^{13}$	273
2	$2C_2H_6 \longrightarrow C_3H_8 + CH_4$	$1.87x10^{11}$	275
3	$C_2H_4 + C_2H_6 \longrightarrow C_3H_6 + CH_4$	$2.57x10^{11}$	253
4	$C_3H_8 \leftrightarrow C_3H_6 + H_2$	$3x10^{10}$	214.7
5	$C_3H_8 \longrightarrow C_2H_4 + CH_4$	$1.03x10^{12}$	211.8
6	$C_3H_8 + C_2H_4 \longrightarrow C_2H_6 + C_3H_6$	$1.267x10^{13}$	247.2
7	$2C_3H_6 \longrightarrow 3C_2H_4$	$1.636x10^{12}$	268.7
8	$2C_3H_6 \longrightarrow 0.3C_{6.5}H_7 + 0.14L + 0.3CH_4$	$3.6x10^{10}$	208
9	$C_4H_{10} \leftrightarrow 2C_2H_4 + H_2$	$3.5x10^{16}$	295.9
10	$C_4H_{10} \longrightarrow C_2H_4 + C_2H_6$	$1.035x10^{15}$	256.6
11	$C_4H_{10} \longleftrightarrow C_4H_8 + H_2$	$1.53x10^{14}$	261
12	$C_4H_8 \longrightarrow 0.41C_{6.5}H_7 + 0.19L$	$1.432x10^{5}$	212.4
13	$C_4H_8 \longrightarrow C_4H_6 + H_2$	$1.182x10^{11}$	209.3
14	$C_2H_4 + C_4H_6 \longrightarrow B + 2H_2$	$8.3x10^{2}$	103.2
15	$C_4H_8 + C_3H_6 \rightarrow T + 2H_2$	$1.38x10^{4}$	140.4
16	$C_4H_6 + C_4H_8 \longrightarrow EB + 2H_2$	$3.613x10^{12}$	246.1
17	$2C_4H_6 \longrightarrow ST + 2H_2$	$1.32x10^{12}$	263.4
18	$C_2H_4 \longrightarrow 0.15C_2H_6 + 0.233C_3H_6 + 0.1C_4H_8$	$3.148x10^{15}$	303.8
19	$C_3H_6 + C_2H_6 \longrightarrow C_4H_8 + CH_4$	$9.673x10^{13}$	291.1
20	$C_3H_6 \longrightarrow C_2H_2 + CH_4$	9	59.38

To determine rate constants as frequency factor and activation energy, least square algorithm was utilized. The objective function clarifies in the equation (3) is used in the algorithm:

$$f = w_1 \sum_i (C_{j\,model} - C_{j\,exp})^2 + w_2 \sum_i (T_{j\,model} - T_{j\,exp})^2 \quad (3)$$

Cjmodel and Cjexp are respectively the reactor outlet molar concentration calculated from model and obtained from experiments. Moreover, Tjmodel and Tjexp are the temperature of different reactor sections fixed or determined in model and experiments. The procedure of investigation of rate constants is demonstrated in figure (1).

As demonstrated in figure 1, the first step of the procedure is generation the initial estimations. These are the initial estimates of rate constants and activation energies of the proposed reaction network .In the second stage, the reactor model is run with the introduced constants to calculate the outlet concentration of different species. In the next step, utilizing the calculated and experimental information the objective functions are investigated. If the objective functions values meet the minimum value, they are reported as the optimum value. Otherwise, the next generation of rate constants are generated and fed to the other steps of the determination procedure.

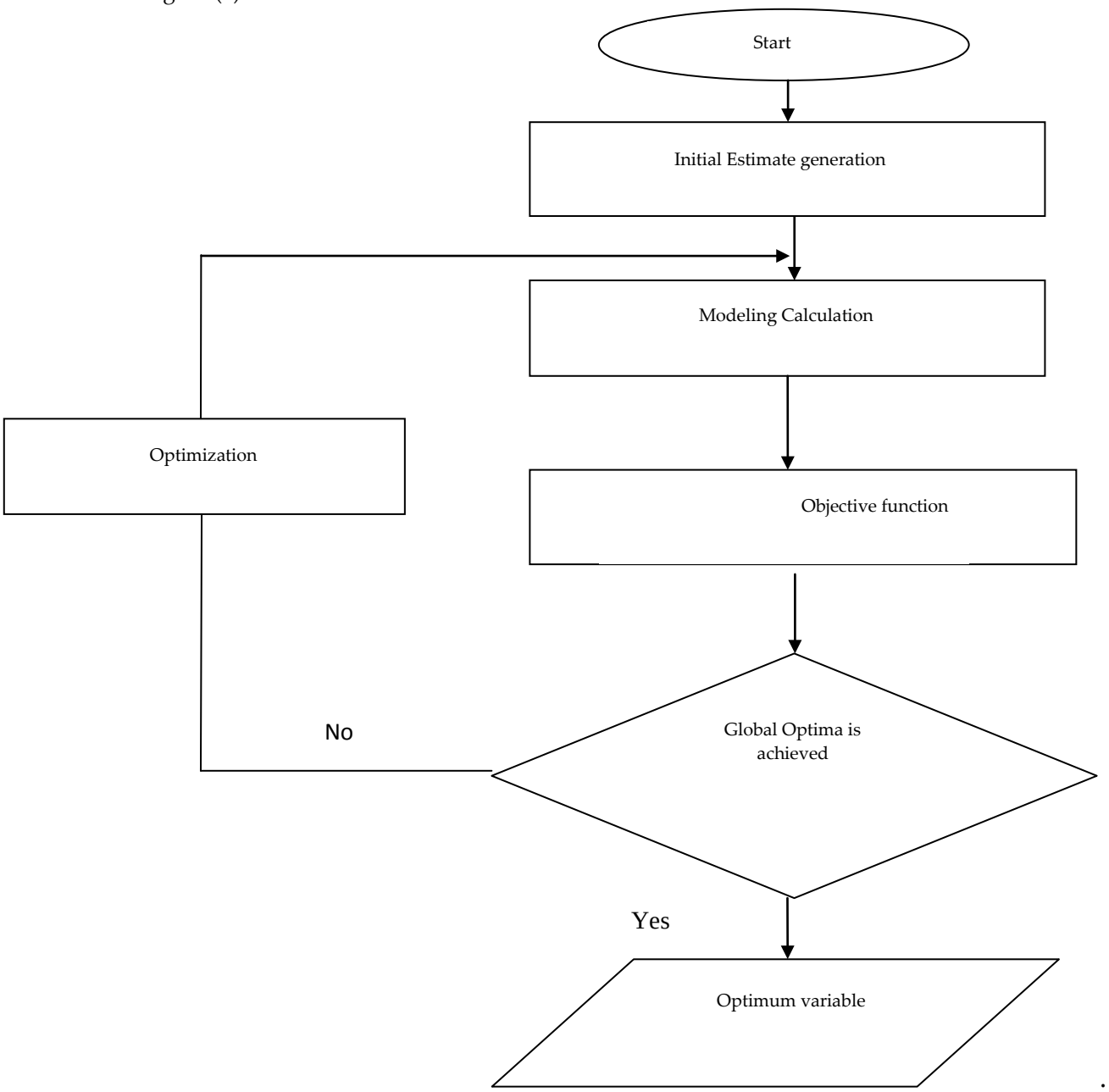

FIG. 1 THE OPTIMIZATION PROCEDURE FOR DETERMINATION OF KINETIC RATE CONSTANTS

Result and Discussion

Based on developed statistical model, the effects of variation of operating variables on coke formation rate are determined and demonstrated in figure(2) to figure(4).In figure(2), the effect of variation of feed flow rate and coil outlet temperature(COT) is clarified. Increasing COT, less than 760(ºC) for stable feed flow rate decreases the coke formation rate. On the other hand, an increment in feed flow rate for stable COT decreases the coke formation rate.

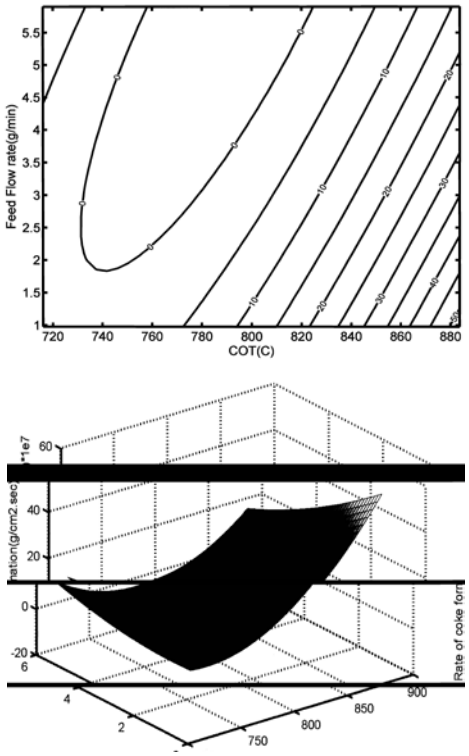

FIG (2) - COKE FORMATION RATE VERSUS FEED FLOW RATE (GR/MIN) AND COIL OUTLET TEMPERATURE (°C) AT CONSTANT STEAM RATIO (GR/GR)

As figure (3) declares, increasing steam ratio with constant operating conditions decreases the coke formation rate. Also, equal increment in steam ratio and COT raises the rate of coke formation with the style like as the position in which only the temperature is increased.

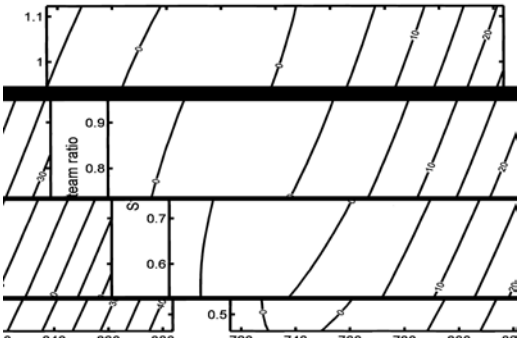

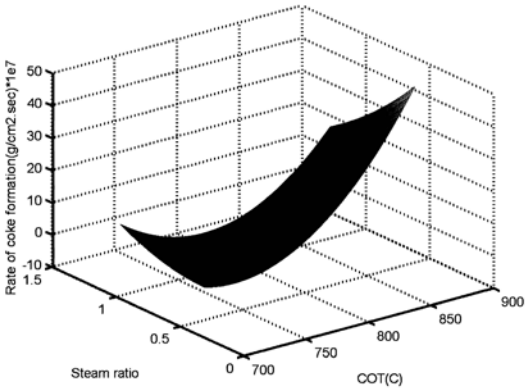

FIG (3) - COKE FORMATION RATE VERSUS COT (°C) AND STEAM RATIO AT CONSTANT FEED FLOW RATE (GR/MIN)

Moreover interaction effect of feed flow rate and steam ratio on coke formation rate can be obtained in figure (4). Indeed, equal increasing of steam ratio and feed flow rate decreases the rate of coke formation.

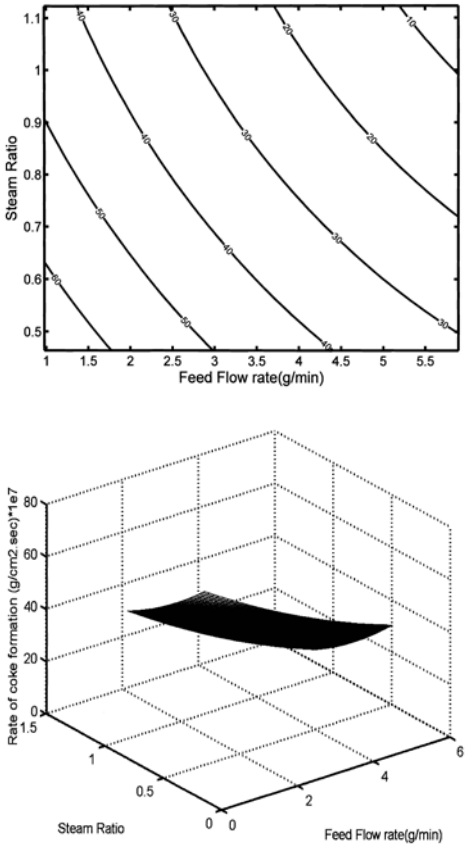

FIG (4) - COKE FORMATION RATE VERSUS STEAM RATIO (GR/GR) AND FEED FLOW RATE (GR/MIN) AT CONSTANT COIL OUTLET TEMPERATURE (°C)

The maximum observable coke formation rate which is equal to $6.62*10^{-6}$ gr/cm^2.sec is observed at the maximum coil outlet temperature, minimum steam ratio and minimum feed flow rate which are respectively equal to 884(ºC), 0.464 (gr/gr) and 0.977 gr/min.

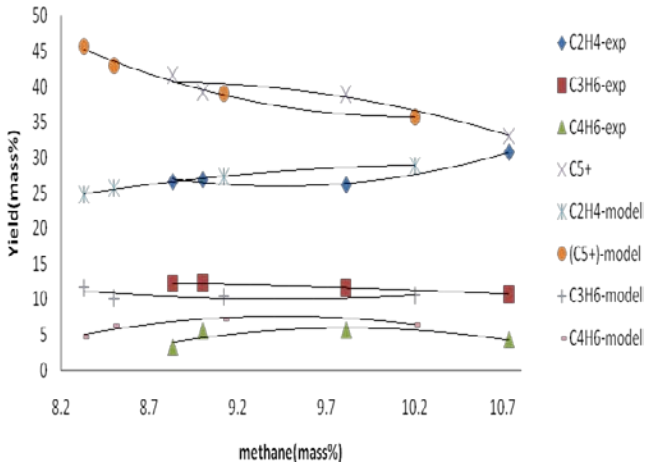

FIG (5) - YIELD OF DIFFERENT PRODUCT VERSUS YIELD OF METHANE

As mentioned above, a molecular reaction network was developed for modeling of steam cracking reactors. Figure (5), demonstrates the effects of the variation of methane yield on the yield of different products. Increasing the yield of methane always decreases the yield of C5+ and increases the ethylene yield. However, the propylene yield has limited variation by increasing the methane yield. Applying the developed statistical and kinetic models together with SQP (Sequential Quadratic Programming) algorithm as a powerful optimization tool, optimization of the pilot plant is conducted. Maximization of net profit of the process is usually suitable objective function in optimization procedure of a chemical process which can be defined as follow:

$$f = income - cost \tag{4}$$

In the above equation, the "income" refers to the price of products. Moreover, "Cost" refers to the production cost, in which the cost of coke regeneration, energy consumption during steam cracking and the cost of consumed water are included in production cost.

Hence, the "income" item mentioned in equation (2) should be introduced as follow:

$$\begin{aligned} income = {} & 6*10^{-4}*mfeed*(1.15*EthyleneYield + \\ & 1.16*PropyleneYield + 0.831*ButadieneYield + \\ & 0.35*ButenesYield + 0.266*Fueloil Yield + 0.575*Lightgas Yield) \end{aligned} \tag{5}$$

The cost of process refers to the cost of consumed water, cost of feed, cost of heat and consumed energy .Cost of water and feed flow rate are encountered in the following relations:

$$cost = 2.64*10^{-4}*m^{0}_{feed}*steam\_ratio + 0.03156*m^{0}_{feed} \tag{6}$$

TABLE 6 PRODUCT VALUED AND OPERATING COSTS [17, 18]

Item	Value
Power($/kWh)	0.06
Feed($/kg)	0.525
Acetylene($/kg)	0.95
Ethylene($/kg)	1.15
Propylene($/kg)	1.16
Butadienes($/kg)	0.352
Deionized water($/kg)	0.0044
Fuel oil($/kg)	0.266
Light gases($/kg)	0.574

The cost of consumed energy is divided into two parts as the consumed energy for olefin production and consumed energy for decoking process. The price of consumed energy for production of olefins is calculated by the following equation:

$$P_1 = \frac{0.216}{\eta} * UA * (T_{skin} - T) \tag{7}$$

In this equation, η, TSkin and T respectively refer to the furnace efficiency, skin temperature of reactor pipe and the temperature of reactive mixture. The cost of decoking is calculated by equation (8);

$$P_2 = P_{2C} + P_{2F} \tag{8}$$

P_{2C} is the cost of compressor consumed energy; P_{2F} is the cost of energy consumption in furnace during the decoking procedure. The consumed energy is calculated by the following equation.

$$P_{2C} = 0.216*Q_{Air}*P_{outlet}*(\frac{P_{inlet}}{P_{outlet}})^{\frac{k''-1}{k''}}*\frac{k}{k-1}[(\frac{P_{ouotlet}}{P_{inlet}})^{\frac{k''-1}{k''}} - 1]\lambda \tag{9}$$

The P_{2F} variable is defined as follow:

$$P_{2F} = P_1 * \lambda \tag{10}$$

λ is the ratio of decoking over olefin production time periods. The defined optimization problem has some constrained. At first, due to the metallurgical limitation, the reactor temperature should not be

exceeded than 890ºC. As the second constrained, the yield of each product have to be in the range of 0% to 100%. And due to the mass continuity rule, the reactor mass inlet flow rate should be equal to the reactor mass outlet flow rate. The result of optimization procedure is calculated and clarified in table7.

TABLE 7 THE RESULT OF OPTIMIZATION

Operating condition	Value
Coil outlet Temperature(ºC)	883
Feed flow rate (gr/min)	6.02
Steam ratio(gr/gr)	0.62
Residence time(sec)	0.3
$Y_{Acetylene}$(%)	1.23
$Y_{ethylene}$(%)	28.23
$Y_{propylene}$(%)	12.33
$Y_{Butadiene}$(%)	4.02
$Y_{Butenes}$(%)	0.98
Y_{LG}(%)	9.70
$Y_{fuel\ oil}$(%)	28.16
Rate of Coke formation (gr/cm2.sec)*10^7	24.32

Determination of optimum temperature profile in reactor is one of great challenges in running of steam cracking process. Three different temperature profiles for three different optimization cases as maximization of ethylene production, maximization of propylene production and maximization of profit are determined and demonstrated in figure(6).

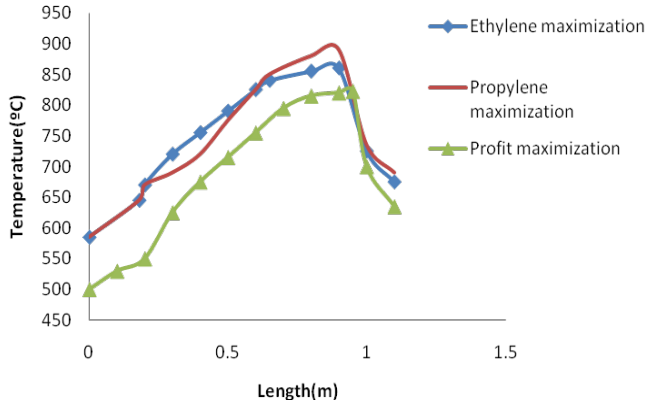

FIG. 6THE OPTIMUM PROFILE FOR MAXIMIZATION OF PROFIT, PROPYLENE AND ETHYLENE AT RESIDENCE TIME AND STEAM RATIO RESPECTIVELY EQUAL TO 0.362 SEC AND 0.88

As demonstrated in the aforementioned figure, Temperature profiles for two optimization cases which are solved to maximize the yield of propylene and ethylene have many similarities. The reactor inlet and outlet temperature are same in both profiles. But, the average reactive mixture temperature for ethylene maximization case is greater than for the propylene maximization challenge. Infact, the rate of temperature increment for the first case is greater than for temperature profile of the second case. The maximum point of temperature profile of the second case is greater than the first one. The third one has many differences from the others. The style of these profiles can be interpreted by the nature of production of the two important olefins as ethylene and propylene. These two olefins are the main primary products which contribute in formation of the secondary products. But propylene has greater role and consequently is more consumed in secondary products. Increment the temperature along the reactor with high rate, raises the possibilities of improvement of secondary reactions that will cause to consumed more propylene. So, reduction of the rate of temperature raising at the inlet reactor regions and maximizing the temperature before sharp declining maximized the yield of propylene. But, since ethylene is produced in primary and some secondary reactions, determination of the operating condition to make little improvement in the secondary reactions may maximize the ethylene production. Moreover, the temperature profile for profit maximization shows several differences from the others. The inlet, average value and the outlet temperatures of this profile are less than the others. Infact, the demonstrated profiles declares that the amount of energy consumption has highlighted effect in the profit of the process.

Conclusions

To evaluate the atmospheric gasoil as a suitable feed stock of steam cracking process, several tests were carried out in a pilot plant. Based on the experimental results, a rigorous kinetic and a statistical model were developed. The results of statistical model proposed that increasing the Temperature could increases the rate of coke formation. While increasing the feed flow rate and steam ratio has inverse effect and could decrease the coke formation rate.

Based on rigorous kinetic model and the experimental results, the yield of main products as ethylene, propylene and butadienes versus the yield of methane as an index of improvement of reaction network were studied. While the yield of ethylene shows increasing trends, the style of C_{5+} yield has decreasing trend and propylene has limited variation. The optimization was carried out to determine the best operating conditions

for profit maximization. To develop the related objective function, the price of product is considered as income and the summation of the price of feed, cost of consumed water and cost of consumed energy is considered as the cost of the process. The results clarified that the maximum observable profit is obtained at the COT, Feed flow rate and steam ratio equal to 883ºC, 6.02gr/min and 0.62 (gr/gr). To determine the effect of reactor temperature profile on the yield of main products and the net profit, optimization was carried out. The results clarified that energy consumption has important effect on the net profit. Moreover, the rate of temperature increment and the value of maximum temperature have important rolls on the maximization of olefin production.

ACKNOWLEDGMENT

The financial support provided by research and development center of National petrochemical company is highly appreciated.

Nomenclature

COT	coil outlet temperature (ºC)
Coef.	coeficient in quadratic model
Tfurnace	temperature of reactor furnace (K)
Tskin	skin temperature of the reactor (K)
XOT	cross over temperature (ºC)
X1	experimental design parameter (feed flow rate (gr/min))
X2	experimental design parameter (steam ratio)
X3	coil outlet temperature (ºC)
Yi	yield of products (mass %)
α	constant coefficient in quadratic model
βij	coefficients in quadratic model
λ	experimental factor for predicting the relationship between decoking time and operating time (hr/hr)

REFERENCES

Dhuyvetter I., Reyniers M. F., Forment G. F, Marin G.B., the Influence of Dimethyle Disulfide on Naphtha Steam Cracking, 40, 4353-4362, 2001

"Ethylene Technology, Process, End Use, manufacturers list, global production and consumption "; www.ynfx.com; 2007

"Ethylene";http://en.wikipedia.org/wiki/Ethylene

F.D. Kopernike, G. Zimmermann, G.C. Reyniers, G.F.Froment," Relative Rates of Coke Formation From Hydrocarbons in Steam Cracking of Naphtha.2.Paraffins,Mono-Di-and Cycloolefins, and Acetylenes", Ind. Eng. Chem. Res.,1993,Vol 32,pp 56-61.

Formation in Steam Crackers for Ethylene Production" Chemical Engineering and Processing, 2002, Vol.41, pp 199-214.

F.Shubo, S.Liming, L.Qiangkun; "A Study on Coke deposition and coking inhibitors during AGO Pyrolysis in pulsed micro reactor system"; Journal of analytical and applied Pyrolysis"; vol.65; PP 301-312.

G.Chan, F.Inal and S. Senkan; "Suppression of Coke Formation in the steam Cracking of Alkanes: Ethane and Propane"; I & EC Research; 1998; vol(37); pp 901-907.

G.Merz; G.Schmidt; D.Kaufmann;"Cracking furnace fundamentals"; Linde Ethylene Technology Seminar; Bahrain; 2003.

Haiyang Cai, Andrzey Kizyeicki, Michael C. Oballa," Coke .

K.M.Saundram; G.F.Froment; "Modeling of thermal cracking kinetic-II Cracking of Iso-Butane, of n-Butane and of mixtures Ethane-Propane and n-Butane";Chemical Engineering science;1977;vol 32;pp 609-617.

K.M. Sundaram, G.F. Froment,' Kinetics of Coke Deposition in the Thermal Cracking of Propane", Chemical Engineering Science, 1979, Vol.34, pp 635-644.

Mohaddecy, R.S., Sadighi, S., Zahedi, S. and Bahmani, M. "LP modeling of Tehran refinery to maximize the net profit", Technical Report, Tehran Refinery (2006).

"Propylene"; http://en.wikipedia.org/wiki/Propene

R. E. Brown; L. E. Reed; G. J. Greenwood; T. P. Harper; M. D. Sharre; US Patent NO:5565087;(1996).

Renjun Zou; "Fundamentals of pyrolysis in Petrochemistry and Technology"; Lewis Pub; 1993.

S.E.Babash, T.N. Mukhian," Effect Coke Inhibition in Pyrolysis Furnaces", PTQ, Autumn1999, pp 113-120.

Tao Ren, Martin Patel and Kornelis Block; "Energy Efficiency and innovative emerging technologies for olefin production"; European Conference on Energy Efficiency in IPPC; 2005.

"The price of different products", http://WWW.nioc.org/publications/fanavari/findex.asp

Zou Ranjun, Lou Qiangkum, Liu Huicai, N. Fenghui," Investigation of Coke Deposition during the Pyrolysis of Hydrocarbon", Ind. Eng. Chem. Res., Vol, 26, pp 2528-2532.

Oil-water Interfacial Tension Effects on Relative Permeability Curves in Low-permeability Reservoirs

Lin Zhao[*1], Ai-Fen Li[2], Xiong-Jun Wu[3], Hao-jun Xie[4], Jin-jie Wang[5], Qian Wang[6]

[*1]School of Petroleum Engineering, China University of Petroleum (East China), Qingdao, P. R. China

[2]School of Petroleum Engineering, China University of Petroleum (East China), Qingdao, P. R. China

[3]Drilling Technology Research Institute, Shengli Petroleum Engineering CO., LTD, Sinopec, Dongying, P. R. China.

[4]School of Petroleum Engineering, China University of Petroleum (East China), Qingdao, P. R. China

[5]School of Petroleum Engineering, China University of Petroleum (East China), Qingdao, P. R. China

[6]Engineering Research Institute, Northwest Oil Field, Urumqi, P. R. China

[*1]zhaolinshiyou@126.com

Abstract

Relative permeability curves of low permeability cores with different permeability were obtained through displacement experiments, including water flooding and surfactant flooding. Changes of the relative permeability curves before and after injecting surfactants with different interfacial tensions were contrasted. The relative permeability curves of water flooding had the following characteristics: relatively narrower two-phase region, lower water relative permeability at residual oil saturation, higher residual oil saturation(37.6%, 39.7% and 40.5%, respectively), and lower ultimate oil recovery(only 37.3%, 27.8% and 23.6%, respectively). While oil/water interfacial tension decreased from 16mN/m to 7.1×10^{-4}mN/m, the two-phase region became wider, and residual oil saturation decreased. At the same time, water relative permeability at residual oil saturation increased, and ultimate oil recovery increased by 13.6%, 15.6% and 16.4% respectively. And the lower the interfacial tension is, the better the effect of enhancing oil recovery is. In general, surfactants have a great application prospect on the oil field development of low and extremely low permeability reservoir, and the oil-water interfacial tension should be reduced as far as possible.

Keywords

Low Permeability; Relative Permeability Curve; Surfactant; Interfacial Tension; Recovery

Introduction

Low permeability reservoirs have the main characters of thin pore throats, large specific surface area, low permeability and strongly Jamin effect (Zeng L.B., Qi J.F., and Li Y.G. 2007). The seepage rule of low permeability reservoirs does not obey the Darcy/s law, and there is a threshold pressure gradient, which is different from that of middle and high permeable reservoirs (Yin D., Gao P., Pu H., and Zhao X. 2010; Zeng B.Q., Chen L.S., and Hao F. 2010). After injecting water, dispersed oil droplets remain in the pores of reservoirs, and cannot pass the minute pores. The oil phase of reservoirs flows by the way of small slugs or drops, instead of continuous flow. When the oil droplets and water droplets pass narrow throats, the injection pressure rises due to resistance produced by Jamin effect.The seepage channel of oil in low permeability reservoirs is very narrow, and the filtrational resistance is very high. Also, the diffusion speed of formation energy is very slow. So the ability to absorb water in the injection wells is quite poor, and the injection pressure is high. The production decreases in a much higher speed in the oil production period. Thus the effect of water flooding in low permeability reservoirs is not good enough to enhance oil recovery.

Recent research shows that surfactants can decrease interfacial tension, and improve the oil/water seepage characteristics, so they can reduce injection pressure and enhance oil recovery (Sun C.H., Liu W.D., and Tian X.C. 2009). The mechanism of surfactant active mainly includes: reducing interfacial tension of oil-water, altering the wettability of rock surface (Adibhatia B., and Mohanty K.K. 2007; Bortolotti V., Macini P., and Srisuriyachai F. 2010; Seethepalli, A., Adibhatla, B., and Mohanty, K. K. 2004.) emulsifying crude oil, increasing the surface charges, conglomerating oil drop, forming oil zone, changing

the rheology of crude oil and so on. At present, many scholars have done a lot of experimental studies about surfactants to improve the development effect of low permeability reservoirs (Adams W.T., and Schievelbein V.H. 1987).

Manrique et al. found that current waterflooding recover was only 40-50% of the OOIP because of microscopic oil trapping and macroscopic bypassing (Mantique E.J., Muci, V.E., and Gurfinkel M.E. 2006). Babadagli suggested the surfactant injection was recommendable in the pre-waterflooded unfractured zones as long as the proper surfactant type was selected. To use a surfactant solution for tertiary recovery, surfactant concentration, type and interfacial tension are important factors (Babadagli T., Al-Bemani A., Boukadi F., et al. 2005). Mohan studied the feasibility of oil recovery by surfactant flooding from an oil-wet carbonate reservoir. The unique features of the subject reservoir were high salinity and low permeability (2-5md). 80% OOIP was recovered using the surfactant which gave low interfacial tension (10^{-3}dynes/cm) in comparison to 60% from water flooding at similar pressure drops (Mohan K. 2009).

Oil/water relative permeability curves can show the relationship between relative permeability of oil-water two-phase and water saturation. A lot of reservoir information, including residual oil saturation, rock wettability, theoretical recovery efficiency, sweep area etc. can be obtained from the curves. Torabzadeh and Handy found that surfactants could be used with injection fluids to increase recovery efficiency of immiscible displacements through reduction of interfacial tension, and the oil-water relative permeability increased by decreasing interfacial tension at given water saturations (Torabzadeh S.J., and Handy L.L. 1984). Liu and Li found that reducing oil/water interfacial tension of low permeability reservoirs could reduce additional capillary resistance, as well enhance flow capacity of injection water, and increase relative permeability of water phase (Liu A.W., and Li X.W. 2006). Wang et al. believed that low interfacial tension could improve the values of oil-water relative permeability, thus making the intersection of oil/water relative permeability curves moves to the right, and decreases residual oil saturation (Wang Y. D., Wang S. H., and Jiang Z. J. 2004). Liu et al. thought that the decrease of oil/water interfacial tension could reduce additional capillary resistance (Liu Q., Dong M., and Ma S. 2006). So dispersed oil drops could flow through throats more easily. Water injection capacity as well as oil recovery could also be improved. To sum up, surfactants have great influence on the two-phase relative permeability and recovery efficiency of low permeability reservoirs. However, there is no certain conclusion for the relationships between the interfacial tension and those parameters of low permeability cores with different permeability.

In this paper, different oil-water relative permeability curves of low permeability cores with different permeability were drew in the course of displacement experiments. And the variations of relative permeability curves under different value of interfacial tension were discussed. Moreover, qualitative and quantitative evaluations of surfactant's ability to enhance oil recovery were conducted.

Materials and Methods

Materials

1) Experiment Materials

• Cores

In this study, natural low permeability cores of Shengli Oilfield were used, and the basic data are listed in Table 1.

TABLE 1 BASIC DATA OF EXPERIMENTAL CORES

Core number	Length /cm	Diameter /cm	Gas log permeability /$10^{-3}\mu m^2$	Porosity /%
Core 5-8	5.90	2.50	33.2	17.58
Core 62-3	5.78	2.51	7.30	15.65
Core 97-2	6.11	2.50	0.52	13.87

• Formation Water

The formation water of Shengli Oilfield was used which had the salinity of 1785mg/L.

• Simulated Oil

Simulated oil was obtained by mixing diesel and crude oil of Shengli Oilfield with the proportion of 4:6, and its viscosity was 2.28mPa•s at 50°C.

Interfacial tension between the formation water and the simulated oil was 16mN/m.

• Surfactant

Surfactant HFYQ-B was selected, and interfacial tensions between 0.2%, 0.25% HFYQ-B and the simulated oil were 0.0092mN/m, 0.00071mN/m, respectively.

• Experiment Apparatuses

Many apparatuses, including TX-500 spinning drop interface tensiometer, reservoir simulation displacement equipment, electronic balance, etc., were applied in the experiments.

2) Experimental Methods

Conduct displacement experiments to get the relative permeability curves of low permeability cores by steady state method and non-steady state method.

Experimental temperature was 50°C. Experiment procedures were as follows. And the flow chart is shown in Fig.1.

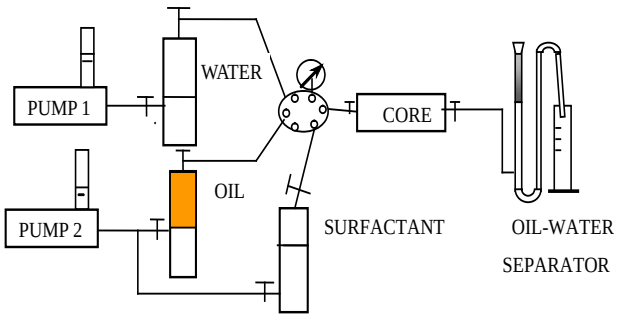

FIG. 1 FLOW CHART OF CORE DISPLACEMENT EXPERIMENTS

(1) Weigh the core after drying it, then vacuumize and saturate it with formation water. Weigh again to calculate the pore volume of the core.

(2) Drive the core with formation water at a constant speed of 0.05mL/min under a temperature of 50°C.

(3) Drive the core with the simulated oil to irreducible water saturation, age 24 hours, then record the volume of oil saturated, last but not the least calculate irreducible water saturation, and effective permeability of oil phase under irreducible water saturation.

(4) Non-steady state method (for cores whose gas permeability is higher than 5×10-3μm2).

- Set a certain pressure at the core inlet, and keep the pressure lower than the steady pressure when the effective permeability of oil phase was measured.
- Drive the core with the formation water. Record the cumulative oil production, cumulative fluid production and their corresponding inlet pressure during the displacement experiment. And record the oil production before water breakthrough time, and the accurate water breakthrough time.
- Calculate the oil/water relative permeability and the corresponding water saturation as well as the water ratio. Then draw the relative permeability curves.

(5) Steady state method (for cores whose gas permeability is lower than 5×10-3μm2)

- Inject the mixture of oil and water at a certain ratio into the core. Record the differential pressure and the flow rate of oil/water after the flow was stable.
- Get the water saturation of core by weight method. And calculate the oil/water effective permeability according to Darcy's equation.
- Then Draw the relative permeability curves.

(6) Wash and dry the core. Repeat the steps (1) ~ (5) of the experiment through changing with surfactants of different interfacial tensions. Likewise, draw the relative permeability curves, respectively.

Results and Discussion

The relative Permeability Curves of Cores with Different Permeability

The displacement experiments were conducted with the formation water, 0.2%HFYQ-B surfactant solution, and 0.25%HFYQ-B surfactant solution, respectively. Three cores were used in these experiments (as shown in Table 1).

Both core 5-8 and core 62-3 were measured by using the unsteady state method. The relative permeability curves of core 5-8 and core 62-3 under different interfacial tensions are showed in Fig.2 and Fig.3, respectively. Core 97-2 was measured by using steady state method. The relative permeability curve of core 97-2 under different interfacial tensions is showed in Fig.4.

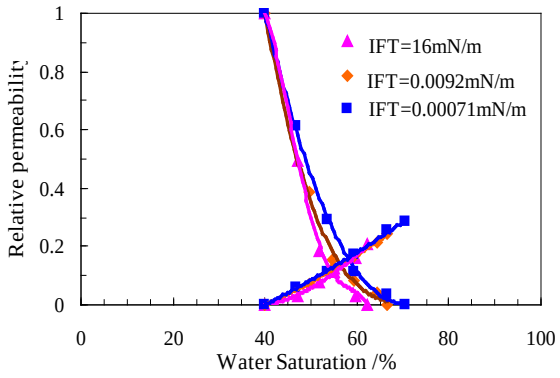

FIG. 2 RELATIVE PERMEABILITY CURVES UNDER DIFFERENT INTERFACIAL TENSIONS

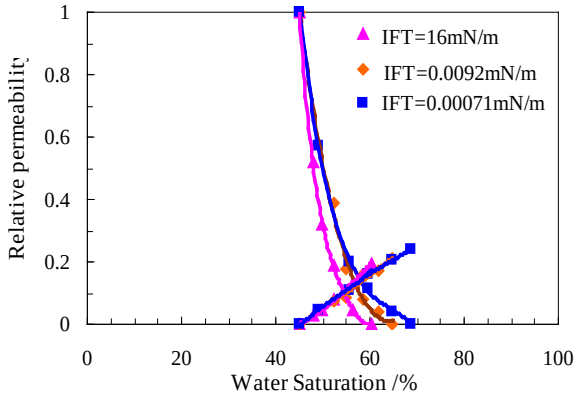

FIG.3 RELATIVE PERMEABILITY CURVES UNDER DIFFERENT INTERFACIAL TENSIONS OF CORE 62-3

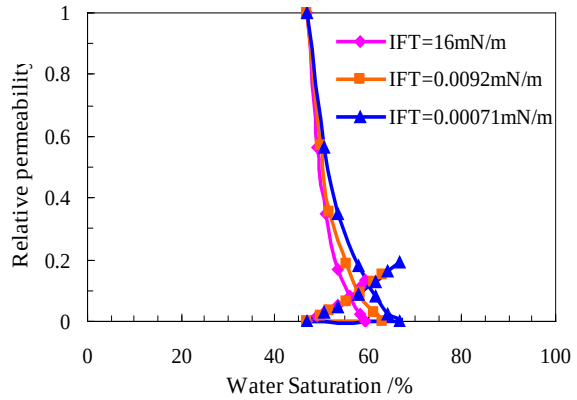

FIG. 4 RELATIVE PERMEABILITY CURVES UNDER DIFFERENT INTERFACIAL TENSIONS OF CORE 97-2

Through analysis of the Fig.2, Fig.3, and Fig.4, one can get the following conclusions:

(1) The two-phase region of relative permeability curves obtained from the displacement experiments using the formation water is quite narrow. And the relative permeability of water phase under the state of residual oil is low. The residual oil saturation of core 5-8, core 62-3 and core 97-2 is high, reaching 37.6%, 39.7% and 40.5% respectively. So the ultimate oil recovery of all the three cores is low, only 37.3%, 27.8% and 23.6% respectively (Table 2).

TABLE. 2 CHARACTERISTICS OF RELATIVE PERMEABILITY CURVES UNDER DIFFERENT FLOODING PATTERNS

Core number	Interfacial tension /(mN/m)	Residual oil saturation /%	Water permeability under residual oil	Ultimate oil recovery /%
Core 5-8	16.000	37.6	0.208	37.3
	0.0092	33.5	0.243	44.2
	0.00071	29.4	0.287	50.9
Core 62-3	16.000	39.7	0.196	27.8
	0.0092	35.1	0.213	36.2
	0.00071	31.1	0.238	43.4
Core 97-2	16.000	40.5	0.185	23.6
	0.0092	36.9	0.199	30.4
	0.00071	33.4	0.214	37.0

There are some reasons for these results as follow:

During the process of water flooding, dispersed oil drops remain in reservoir pores and cannot flow through minute pores. The oil phase flow in the state of small slug or dispersed drops, instead of a continuous state. When oil drops or water drops flow through narrow throats, the injection pressure would increase because of Jamin Effect. And water lock effect occurs during the operation in oil wells. The formation energy spreads slowly in low permeability reservoirs. The recovery of water flooding is low as a result.

(2) With the decrease of interfacial tensions of oil-water, the two-phase region increases, the permeability of water phase under the state of residual oil increases, and the residual oil saturation decreases. So the ultimate oil recovery is improved. For instance, when interfacial tension drops from 16mN/m to 7.1×10^{-4}mN/m, residual oil saturation of core 5-8, core 62-3 and core 97-2 decreases by 8.2%, 8.6% and 7.1% respectively, and ultimate oil recovery of core 5-8, core 62-3 and core 97-2 increases by 13.6%, 15.6% and 16.4% respectively (Table 2).

There are some reasons for these results as follows:

Surfactant can reduce interfacial tension and capillary resistance, make oil bead deform easily, and decrease the power on which oil droplets were emitted through the pore throat depending. It is easier for oil drop to change the shape of itself and flow through the throat. The residual oil saturation decreases greatly. And amphipathy of surfactant enables itself to absorb the surface of boundary layer of core, which can reduce the thickness of boundary layer liquid so that throat volume becomes lager and flow resistance decreases. Moreover, surfactant can not only reduce the adhesive resistance of oil film on the rock surface, but also emulsifies the oil film and impels it to fall off from the surface. Meanwhile, owing to the reduction of residual oil the flowing space of water phase increases gradually, so sweep efficiency is becoming larger, and the relative permeability of water phase becomes higher. In all, the lower interfacial tension is, the higher the extent of enhancing oil recovery is.

However the residual oil saturation has not dropped to zero when treated with surfactant of ultra-low interfacial tension. Analysis indicates that the emulsified oil droplets in narrower pore space may be displaced through the pore throat only when the lower interfacial tension is reached. In addition, the sweep volume of surfactant solution is limited. It is difficult

for residual oil saturation of low permeability cores to drop to a very low degree as a result. Therefore, further study should be focused on the lower oil-water interfacial tension and the sweep efficiency of surfactant solution.

(3)The relative permeability of oil phase increases with the decrease of interfacial tension, but the relative permeability of water phase (within endpoint) is not affected. Analysis shows that surfactant lowers the resistance of oil droplet flowing through the pore throat caused by Jamin effect, and increases the relative permeability of oil phase. On the other hand, the oil beads are produced from small pores of low permeability cores, so more and more residual oil begin to flow. The increase of flowing space of oil phase lead to the increase of oil relative permeability. However, the water permeability is not changed.

Comparison of Various Relative Permeability Curves

For the low permeability cores with different permeability, the relationship of residual oil saturation with oil-water interfacial tension is drawn in Fig.5. And the relationship of ultimate oil recovery with oil-water interfacial tension is drawn in Fig.6.

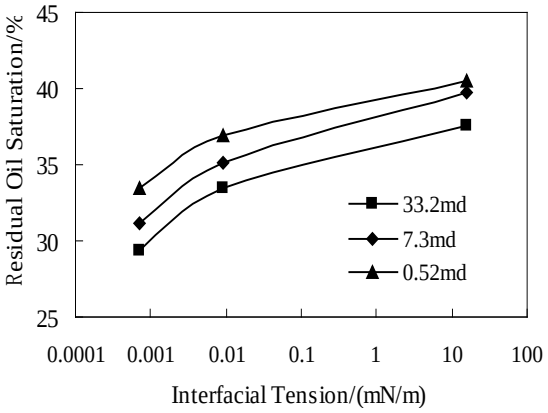

FIG. 5 CURVES OF RESIDUAL OIL SATURATION WITH PERMEABILITY OF CORE

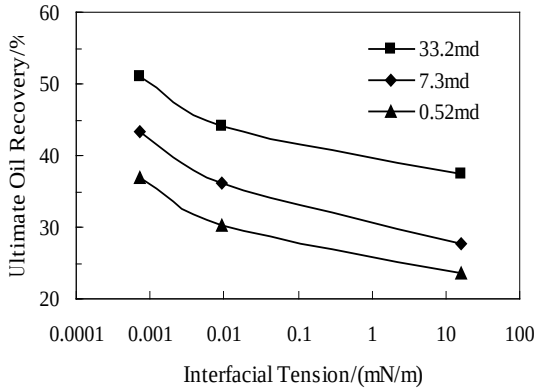

FIG. 6 CURVES OF ULTIMATE OIL RECOVERY WITH PERMEABILITY OF CORE

As shown in Fig.5, not only, residual oil saturation increases with the increase of oil-water interfacial tension, but also it increases with the decrease of permeability of the core.

Similarly, there is inverse relationship between the ultimate oil recovery and oil-water interfacial tension or permeability of the core in Fig.6.

Analysis, in general, the less the permeability of the core is, the narrower the average throats radius in core is, and the more complex the distribution of pore throat. The snap-off of oil resulting from the minute pore and throat is more serious, and the more dispersed oil drops remain in reservoir pores. So the Jamin effect is increased, and oil beads are more difficultly produced, resulting in higher residual oil saturation and lower ultimate oil recovery.

The relationship of water relative permeability at residual oil saturation with oil-water interfacial tension is drawn in Figure 7.

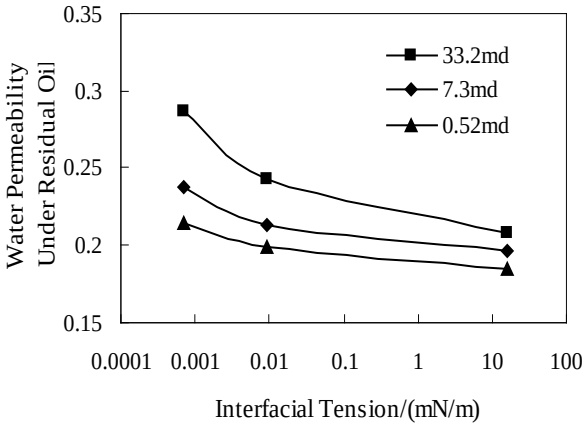

FIG. 7 CURVES OF WATER PHASE PERMEABILITY UNDER RESIDUAL OIL WITH PERMEABILITY OF CORE

As shown in Figure 7, not only, water relative permeability at residual oil saturation decreases with the increase of oil-water interfacial tension, but also it decreases with the decrease of permeability of the core. Analyzing its reason, the lower the permeability of core is, the higher the residual oil saturation is. So the flowing space of water phase is much smaller, and the amount of oil droplets trapped at pore throats is increased, and Jamin effect is increased. As a result, the water relative permeability at residual oil saturation is in a smaller level.

Conclusions

The relative permeability curves of water flooding had the following characteristics: relatively narrower two-

phase region, lower water relative permeability at residual oil saturation, higher residual oil saturation, and lower ultimate oil recovery.

At the same oil/water interfacial tension, residual oil saturation, water relative permeability at residual oil saturation and ultimate oil recovery decreased with the decrease of permeability of core.

With the decrease of oil/water interfacial tension, the two-phase region became wider, residual oil saturation decreased, water relative permeability at residual oil saturation increased, and ultimate oil recovery increased.

Moreover, the relative permeability of oil phase increases with the decrease of interfacial tension, but the relative permeability of water phase (within endpoint) is not affected.

ACKNOWLEDGMENT

The authors thank the Key Project of China Petroleum & Chemical Corporation Foundation (Grant No.P06074) for financial support of this research. The authors also acknowledge reviewers for pertinent revision suggestions.

REFERENCES

Adams W.T., and Schievelbein V.H. Surfactant Flooding Carbonate Reservoirs. SPE Reservoir Engineering 619-626,1987.

Adibhatia B., and Mohanty K.K. Simulation of surfactant-aided gravity drainage in fractured carbonates. SPE Reservoir Simulation Symposium, Houston, February 26-28, 2007.

Babadagli T., Al-Bemani A., Boukadi F., et al. A Laboratory Feasibility Study of Dilute Surfactant Injection for the Yibal Field, Oman. Journal of Petroleum Science and Engineering 48 (1): 37-52, 2005.

Bortolotti V., Macini P., and Srisuriyachai F. Wettability index of catbonatic reservoirs and EOR: laboratory study to optimize alkali and surfactant flooding. International Oil and Gas Conference and Exhibition in China, Beijing, June 8-10, 2010.

Liu A.W., and Li X.W. Two phase percolation characteristics in low permeability reservoirs and its influence. Journal of Oil and Gas Technology, 28(3):325-327, 2006.

Liu Q., Dong M., and Ma S. Alkaline/surfactant flood potential in western Canadian heavy oil reservoirs. SPE/DOE Symposium on Improved Oil Recovery, Tulsa, April 22-26, 2006.

Mantique E.J., Muci, V.E., and Gurfinkel M.E. EOR field experiences in carbonate reservoirs in the United States. SPE/DOE Symposium on Improved Oil Recovery, Tulsa, April 22-26, 2006.

Mohan K. Alkaline surfactant flooding for tight carbonate reservoirs. SPE Annual Technical Conference and Exhibition, New Orleans, October 4-7, 2009.

Seethepalli, A., Adibhatla, B., and Mohanty, K. K. 2004. Wettability Alteration During Surfactant Flooding of Carbonate Reservoirs. SPE 89423.

Sun C.H., Liu W.D., and Tian X.C. An Alkaline/Surfactant System for Injection Well Stimulation in Low Permeability and High Temperature Oil Reservoirs. Oilfield Chemistry 26(4):419-421,2009.

Torabzadeh S.J., and Handy L.L. The effect of temperature and interfacial tension on water/oil relative permeabilities of consolidated sands. SPE Enhanced Oil Recovery Symposium, Tulsa, April 15-18, 1984.

Wang Y. D., Wang S. H., and Jiang Z. J. The influence of temperature and interfacial tension on oil-water relative permeability. Oil Gasfield Surface Engineering, 23(4):11-12, 2004.

Yin D., Gao P., Pu H., and Zhao X. Investigation of a new simulator for surfactant floods in low permeability reservoirs and its application in Chao-522 field, 2010 update. SPE EOR Conference at Oil & Gas West Asia, Muscat, April 11-13, 2010.

Zeng B.Q., Chen L.S., and Hao F. Experiment and mechanism analysis on threshold pressure gradient with different fluids. The 34th Annual SPE International Conference and Exhibition, Calabar, Nigeria, July 31-Aug 7, 2010.

Zeng L.B., Qi J.F., and Li Y.G. The Relationship Between Factures and Tectonic Stress Field in the Extra Low-permeability Sandstone Reservoir at the South of Western Sichuan Depression. Journal of China University of Geosciences 18M:223-231, 2007.

Lin Zhao (China, 1984-) majored in oilfield applied chemistry and obtained a master degree of applied chemistry in Yangtze University at 2009, which is in Jingzhou city, Hubei province, China.

She current studies for a doctor degree of petroleum development engineering in School of Petroleum Engineering at China University of Petroleum since Sept 2009, which is in Qingdao city, Shandong province, China. She is major in oilfield chemistry and enhanced oil recovery; the published articles were as follows:

[1] Lin Zhao, Aifen Li, Kai Chen, et al. Development and evaluation of foaming agents for high salinity tolerance. Journal of Petroleum Science and Engineering, 81: 18-23, 2012.

[2] Zhao Lin, Li Aifen, Li Huihui et al. Evaluation on interfacial properties and displacement effect of tri-quaternary ammonium salt. Petroleum Geology and Recovery Efficiency, 19(1):72-74, 2012.

[3] Xiongjun Wu, Lin Zhao, Xiaojun Wang, et al. Synthesis and applications of Tri-quaternary ammonium salt Gemini surfactant. Journal of Dispersion Science and Technology, 34(1):106-110, 2013.

Ai-Fen Li (China, 1962-) majored in oilfield chemistry and enhanced oil recovery and obtained a doctor degree of petroleum development engineering in School of Petroleum Engineering at China University of Petroleum at 2002, which is in Qingdao city, Shandong province, China.

She is working as a lecture in School of Petroleum Engineering at China University of Petroleum since Sept 1998, which is in Qingdao city, Shandong province, China. She is major in oilfield chemistry and enhanced oil recovery; the published articles were as follows:

[1] Li Ai-fen, Chen Kai, Zhao Lin, et al. Optimization and visualization of the injection patterns of foam system. Journal of Xi'an Shiyou University (Natural Science Edition), 26(5):49-52, 2011.

[2] Li Ai-fen, Zhang Dong, Yao Jun, et al. Physical simulation of waterflooding in fractured-vuggy unit. Journal of China University of Petroleum, 36(2):130-135,2012.

[3] Li Ai-fen, Fan Tian-you, Zhao Lin. Experimental study of spontaneous imbibition in low permeability core fractured reservoir. Petroleum Geology and Recovery Efficiency, 18(5): 67-69,2011.

Xiong-Jun Wu (China, 1984-) majored in oilfield chemistry and drilling fluid and completion fluid and obtained a doctor degree of oil and gas well engineering in School of Petroleum Engineering at China University of Petroleum at 2012, which is in Qingdao city, Shandong province, China.

He is working for Drilling Technology Research Institute, Shengli Petroleum Engineering CO., LTD, Sinopec since July 2012, which is in Dongying city, Shandong province, China. He is major in oilfield chemistry and drilling fluid and completion fluid; the published articles were as follows:

[1] Xiongjun Wu, Lin Zhao, Xiaojun Wang, et al. Synthesis and applications of Tri-quaternary ammonium salt Gemini surfactant. Journal of Dispersion Science and Technology, 34(1):106-110, 2013.

[2] Xiong-Jun Wu, Guan-Cheng Jiang, Xiao-Jun Wang, et al. Prediction of reservoir sensitivity using RBF neural network with trainable radial basis function. Neural Computing and Applications, 22(5):947-953, 2013

Hao-Jun Xie (China, 1988-) majored in petroleum engineering and obtained a bachelor degree of petroleum engineering in China University of Petroleum at 2007, which is in Qingdao city, Shandong province, China.

He current studies for a master degree of petroleum development engineering in School of Petroleum Engineering at China University of Petroleum since Sept 2010, which is in Qingdao city, Shandong province, China. He is major in oilfield chemistry and enhanced oil recovery.

Jin-Jie Wang (China, 1987-) majored in petroleum engineering and obtained a bachelor degree of petroleum engineering in China University of Petroleum at 2007, which is in Qingdao city, Shandong province, China.

She current studies for a master degree of petroleum development engineering in School of Petroleum Engineering at China University of Petroleum since Sept 2010, which is in Qingdao city, Shandong province, China. She is major in oilfield chemistry and enhanced oil recovery.

Qian Wang (China, 1984-) majored in oilfield chemistry and enhanced oil recovery and obtained a master degree of petroleum development engineering in School of Petroleum Engineering at China University of Petroleum at 2010, which is in Qingdao city, Shandong province, China.

She is working for Engineering Research Institute of Northwest Oil Field of China National Petroleum Corporation since July 2010, which is in Urumqi city, Sinkiang province, China. And also she is major in oilfield chemistry and enhanced oil recovery.

Complete and Cost-Effective Approach for Diagnosing Formation Damage and Performing Successful Stimulation Operations

Mahmoud Abu El Ela*1

Faculty of Engineering, Cairo University, Cairo, Egypt

*1mahmoud.abuelela@WorleyParsons.com

Abstract

This paper presents and describes a comprehensive and cost-effective approach to diagnose and treat the formation damage problems. The proposed approach consists of systematic steps: recognition of the immediate problem; data collection, analysis and integration; identification of the source of the formation damage problem; assessment of the formation damage; identification of the proposed treatment techniques; evaluation of all options; selection of the best stimulation technique; stimulation process design, implementation of the plan; and evaluation and analysis of the results. Application of such approach in an oil producing well (case study from the Gulf of Suez area) of an international joint venture company in Egypt achieved oil production rate of 560 bbl/day after complete mud loses during the drilling operations. Such study is an original contribution to the knowledge of diagnosing and solving formation damage problems.

Keywords

Acidizing; Formation Damage; Acidizing Operation Design; Stimulation; Matrix Acidizing; Acidizing Treatment; Successful Stimulation Operations

Introduction

The formation damage can be described as any process that causes a reduction in the productivity of an oil and gas producing formation, or a reduction in the injectivity of a water or gas injection well [Civan, 2000]. The formation damage is categorized by the mechanism of its creation as either natural or induced as shown on Fig. 1 [Hill et al., 2000; Ali, 2011]. Natural damages are those that occur primarily as a result of producing the reservoir fluid. Induced damages are the result of an external operation that is performed on the well such as a drilling or injection operations.

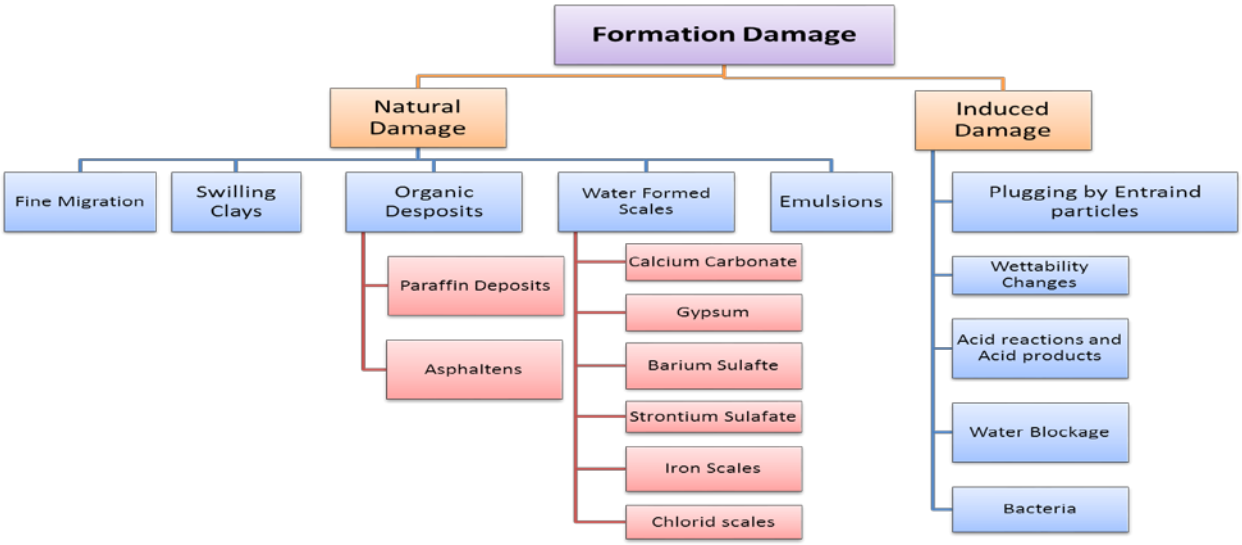

FIG. 1 FORMATION DAMAGE CLASSIFICATIONS

The stimulation processes are used to remove the formation damage and enhance the property value by the faster delivery of the petroleum fluid and/or to increase ultimate economic recovery.

Diagnosing and Solving of the Formation Damage Problems

The main objective of this work is to present a complete plan and cost-effective approach to diagnose and treat the formation damage problems. As shown in Fig. 2, the proposed plan incorporates the following steps:

1. Recognition of the immediate problem
2. Data collection, analysis and integration
3. Identification of the formation damage source
4. Assessment of the formation damage
5. Identification of the proposed treatment techniques
6. Evaluation of all options
7. Selection of the best stimulation technique
8. Stimulation process design
9. Implementation of the plan
10. Evaluation and analysis of the results

Recognition of the Immediate Problem

The formation damage problem is recognized, when the well is producing with low productivity relative to what they are capable of producing and then evaluating possible mechanical problems in these wells. Geology, petrophysics and reservoir engineering play important roles in quantifying the productive potential of a given well. Once a well is diagnosed as underperforming, the reasons must be determined.

Data Collection, Analysis and Integration

All available information on the well such as well logs and records, reservoir characteristics and information on the completion and previous workovers should be collected and analyzed. There are four main categories of data to study the reasons of the low productivity and/or low injectivity:

1. Wellbore data such as wellbore dimensions, deviation data, tubular and completion data
2. Reservoir data such as reservoir properties (pressure, temperature, etc.), rock properties, and lithology for the zone of interest
3. Reservoir fluids data such as fluid properties (viscosity, compressibility, density, etc.)
4. Well history data such as history of drilling, completion, stimulation, workover, injection, and withdrawal. The historical information is the key to identifying potential formation damage mechanisms.

All of these data must be assessed before damage mechanisms can be identified and/or treatments are recommended. Data collection, analysis and integration programs require a great deal of effort, scrutiny and innovation. The key steps are (1) plan and organize, (2) collect and analyze, and (3) integrate and store. This approach addresses a general framework of optimizing the data analysis process.

Identification of the Formation Damage Source

Once it has been established that a well is producing below its potential, an assessment must be made to determine the source of the problem: formation damage or mechanical problem. Once mechanical reasons are eliminated as a potential cause of poor production, the wells become stimulation candidates.

Diagnosis can be based on a (1) review of the well and field history, (2) analyses of samples of plugging material recovered from the field, and (3) knowledge of formation mineral and fluid (e.g., water and oil) properties, as well as pressure testing and logging evaluation [Wang, 2009].

Assessment of the Formation Damage Problem

Damage source identification is an essential task prior to treating fluid selection and treatment design. Damage is characterized using the results of the laboratory tests, logging techniques and well history. Detailed study is necessary to develop a list of suspected damages from the available data. Multiple types of damage are normally suspected and are all considered when designing the treatment. Formation damage identification and investigation include types of damage, location of damage, extent and screening of damage, and effect of damage on well production or injection [Allen, 1973; Beadie, 1995].

There are a few logging techniques available to estimate the invasion profile as a result of mud filtrate invasion, presumably causing formation damage. For a vertical well drilled with a conductive mud, an invasion profile may be computed from resistivity logs.

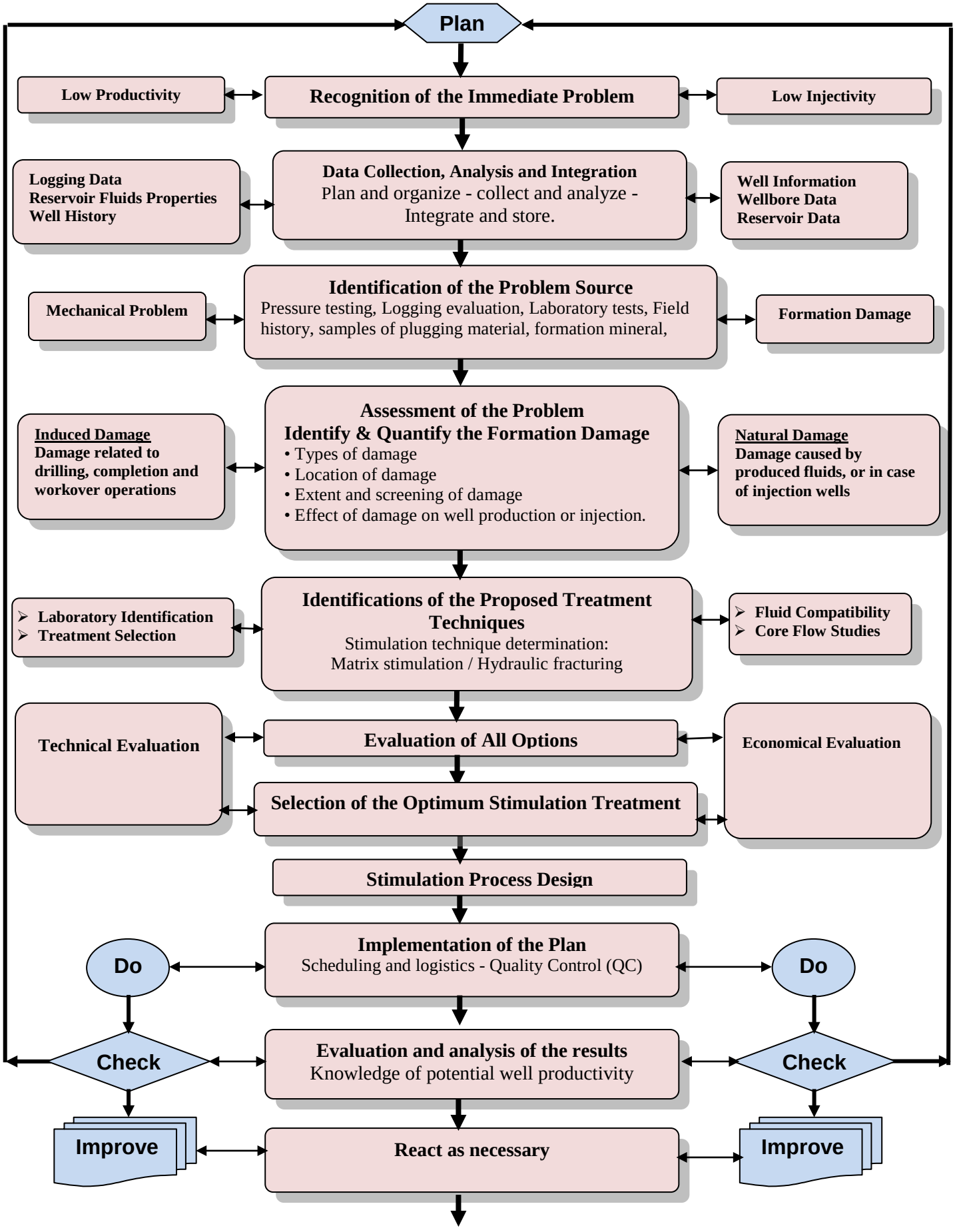

FIG. 2 PLAN FOR DIAGNOSING AND SOLVING OF THE FORMATION DAMAGE PROBLEMS

Resistivity logs provide resistivity measurements at several depths of investigation. Provided that there is a resistivity contrast between the mud filtrate and virgin formation fluid, each resistivity measurement reflects how much the formation fluid is displaced by mud filtrate. The resulting invasion profile does not strictly correlate with a drilling-induced damage profile, but it is a reasonable first-order estimate. This technique can be extended to non-vertical wells by including the effect of dip between the wellbore and the formation.

Another method to estimate the depth of invasion, and thus the drilling-induced damage profile, is the use of TDT (Thermal Decay Time) logs. These record the rate of decay of a thermal neutron population following an emission of high-energy neutrons by the down-hole generator. Some formation elements, primarily chlorine, have a very high capacity to absorb neutrons. Since chlorine is primarily associated with formation water, the TDT log resembles the usual open hole resistivity logs, and therefore gives an indication of the invasion profile.

In some cases, it may be useful to conduct laboratory compatibility tests of the completion or drilling fluids and the formation fluid or rocks. Such tests can help in developing understanding of the problem in the current well and lead to corrective action.

In many cases, it is not possible to characterize the formation damage completely. If the diagnosis is uncertain, it is recommended to prioritize the probable causes and design a treatment for the most probable scenarios.

Identifications of the Proposed Treatment Techniques

Once the cause of formation damage and the location of the damage are known, then one can select the optimum fluid and design the best treatment to remove the damage. Table 1 lists the damage types and remedial recommendations for comparison to the condition and characteristics of the candidate well [Ali, 2011].

The detailed analysis of formation cores is required to design the damage removal treatment. Conventional cores are recommended to complete the analysis because sidewall cores can be contaminated with drilling fluids and may not be representative of the formation. If sidewall cores are used, the analysis should be conducted on duplicate cores.

The formation mineralogy is an important parameter affecting stimulation success. Therefore, the analytical techniques (X-ray diffraction and thin-section analysis) are used to characterize the formation mineralogy.

Matrix treatments are usually used to remove the damage chemically, restoring a well to its natural productivity. Matrix stimulation is accomplished by injecting a fluid (e.g., acid or solvent) to dissolve and/or disperse materials that impair well production in sandstones or to create new, unimpaired flow channels between the wellbore and a carbonate formation. The most common matrix stimulation treatment is acidizing, in which an acidic solution is injected to dissolve minerals in the formation. More than 40,000 acid treatments are pumped each year in oil and gas wells [Ali, 2011]. These treatments typically involve small crews and minimal equipment. The next most common fluids are organic solvents aimed at dissolving waxes, paraffin, asphaltenes or other organic damaging materials.

In some instances, chemical procedures may not be effective or appropriate, and hydraulic fracture operations are used to bypass the damage. This is achieved by producing a high conductivity path through the damage region to restore wellbore contact with undamaged rock. Hydraulic fracture operations may be performed on a well for one (or more) of three reasons [Smith and Shlyapobersky, 2000]:

1. to bypass near-wellbore damage and return a well to its “natural” productivity
2. to extend a conductive path deep into a formation and thus increase productivity beyond the natural level
3. to alter fluid flow in the formation: In this case, fracture design may affect and be affected by considerations for other wells (e.g., where to place other wells and how many additional wells to drill). The fracture becomes a tool for reservoir management.

Hydraulic fracturing with acid (usually hydrochloric acid [HCl]) is an alternative to propped fractures in acid-soluble formations such as dolomites and limestone. The major difference between acid and propped fractures is that conductivity is obtained by etching the fracture faces instead of using a proppant to prevent the fracture from closing. Acid fracturing may be

TABLE 1 CAUSES OF FORMATION DAMAGE AND THE REMEDIAL RECOMMENDATIONS

Operation	Causes of formation damage	Accelerating factors	How to cure the damage
Drilling	- mud filtrate invasion - mud solids invasion - sealing of pores and flow tunnels by the troweling action of the bit, drill collars and drill pipes - plugging by rock cuttings	- high permeability formation - water-based mud - abrupt reduction in salinity - drilling with high water loss - bentonite mud - strongly overpressured drilling - high solids mud	- backflush - acid wash, matrix acidizing
Running casing and cementing	- plugging/blockage of pore space by mud or cement solids - filtrate invasion - chemical reactions with cement additives and spacers	- high-permeability formations	- deep perforations - matrix Acidizing, acid wash
Perforating	- plugging of perforations and formation with debris - compaction of pores around perforations	- use of low performance or expendable guns - perforate overbalanced in drilling mud	- backflow - acidizing
Running completion string	- plugging by solids from completion fluids and diverting agents - filtrate invasion - dissolution of rock cementing material	- overbalanced conditions with damaging completion fluids - improper bridging materials - high-permeability formation - uncleaned wellbore and production equipment	- acid treatment - solvent wash - same as for
Production	- fines movement - clay migration - condensate and water blockage - deposits of salt crystals, wax, and paraffin - hydrate and emulsions forming	- high production rates - increase in water/oil ratio - pressure decrease - communication with water zones - poor gravel-packing or sand-control measures	- acidizing - chemical treatments
Gravel packing	- invasion of filtrate from gravel-pack slurries - invasion of solids and contaminations - mixing of gravel with formation sand - plugging by diverting agents	- variation of permeability along the producing interval - nonuniform sand - clay-rich sand	- Acidizing (through the gravel pack) - replace the gravel pack
Acidizing	- insoluble precipitates - iron precipitation in the wellbore - plugging of solids coured from the tubing	- incompatibility between acid, acid additives and formation materials - damaging diverting agents - large variations in permeability	- re-acidize with proper additives
Fracturing	- plugging by formation fines or damaged by gelled frac fluids	- poorly designed frac	- soak with a gel breaker
Workover	- residual cement plugging - plugging by wireline loosened iron scale or paraffin from tubing - plugging by metallic particles resulting from casing repair operations - damaging workover fluids - damaging bridging materials	- operate at overbalanced conditions - high-permeability formation - large variation in permeability - uncleaned wellbore - use of corrosion inhibitors or emulsion breakers	- acid stimulation - chemical treatment

preferred operationally because the potential for unintended proppant bridging and proppant flow-back is avoided. However, designing and controlling the depth of penetration of the live acid into the formation and the etched conductivity are more difficult than controlling proppant placement. Acid penetration is governed by the chemical reaction between the rock and the fracturing fluid (as opposed to a simple mass balance in propped fractures), and conductivity is determined by the etching patterns formed by the reacting acid (as opposed to being a property of the proppant under a given stress). In both cases, acid fracturing introduces a dependence on rock properties that is not present in propped fracturing. In addition, the properties that acid fracturing design and control depend on are usually

more difficult to determine than other formation properties.

Evaluation of All Options

Because the whole purpose of stimulation is to increase the value of the producing property through an accelerated production rate or increased recovery, economics should be the driver in deciding whether to conduct the stimulation, what type of stimulation to do and which various aspects of the treatment to include.

Selection of the Optimum Stimulation Treatment

Selection of the optimum method should depend on the technical and economical evaluation of the previous fields' applications.

Stimulation Process Design

Most treatments are currently based on empirical rules of thumb. Key parameters in treatment design are the placement technique, chemical selection and soak time. Mechanical assemblies such as packers, bridge plugs, spring-loaded "spot control" valves and coiled tubing can be used to ensure proper placement. This is critical in minimizing the volume of treating fluid.

Treatment fluid selection is an important step in the engineering process. Multiple fluids (fluid systems), composed of base fluids and additives, are selected on the basis of lithology, damage mechanism and well condition. Each fluid in the treating schedule serves a special purpose. The main treating chemicals fall into the following categories [Thomas and Morgenthaler, 2000]:

- solvents to remove organic deposits (such as paraffin)
- oxidizers to remove damage from polymers
- scale removers to remove sulfate or oxide scales
- acids to remove carbonate and oxide scales, break polymer residues or stimulate carbonate formations
- hydrofluoric acid (HF) to remove aluminosilicate damage (primarily clays) from sandstone formations.

The pumping schedule includes the treating fluid and diverter sequence and the injection rate of each stage. It is generated using empirical rules based on previous field experience or computers.

Proper placement of the treatment fluid over the whole pay zone is required for successful treatment. Five main diversion techniques can be used to improve fluid placement in carbonate acidizing: packers, ball sealers, particulate diverters, foam diversion and self-diverting acid. In large intervals (e.g., horizontal wells) some of these techniques can be combined with the use of coiled tubing.

Implementation of the Plan

The scheduling and logistics along with the site preparation is the first step in the implementation of the treatment operation. Operational constrains and operation stimulation program are reviewed and considered. Materials must be monitored to ensure that they meet the specifications of the design, equipment must be maintained to perform properly, and personnel on site must understand and execute their assigned roles. Quality control (QC) testing and training should be documented as standard practices [Brannon et al., 1987].

Evaluation and Analysis of the Results

After implementing the treatment method, the production rate is regularly observed to realize the success rate of the recommended treatment method and to determine whether the formation damage problem was solved or not?

The analysis of the results of the treatment method indicates whether the treatment requires modification and helps to improve future designs in similar situations.

Case Study: Well I in Nukhul Formation

An international joint venture company in Egypt is currently progressing a development plan in the Gulf of Suez area. The company applied similar approach to solve formation damage problem in one of the development wells "Well I" in Nukhul formation. The recommended remedial actions succeeded to put the well on production with an oil production rate of 560 bbl/day after complete mud loses during the drilling operations. It should be highlighted that the author of this paper (who proposed the above mentioned approach) has not participated in the preparation and the execution of the acid stimulation job of the presented case study.

Well I was drilled to represent additional drainage point for Nukhul reservoir formation. Nukhul formation is characterized by the following:

- It is represented by conglomerates and beach deposits.
- It includes three main pay zones (Nukhul A, B, and C). Two interlayers, represented by strongly cemented siltstone, separate Nukhul A from Nukhul B and Nukhul B from Nukhul C. The uppermost fan sequence (Nukhul A) is capped by another strongly cemented siltstone interval.
- Formation temperature is 205°F.
- Formation pressure ranges between 2700 to 3000 psi at datum level (8600ft).
- Fracture gradient is 0.55 psi/ft.
- Wells history in the same area indicates that severe drilling fluid losses are occurred while penetrating the pay zones of Nukhul formation
- The average productivity of offset wells in Nukhul formation ranges between 400 to1000 bbl/d (65 to160 m3/day) with a water cut of 15%. (productivity index of the offset wells is about 1 bpd/psi)..

During the drilling of Well I with oil base mud, it was observed that severe drilling fluid losses were occurred while penetrating the pay zone. Therefore, loss of circulation material was pumped to control the mud losses. Unfortunately, the mud losses were continued and the decision was taken to side track the well. Well I was drilled and completed with a measured depth of 11942 ft (3640 m). The well logs (Fig. 3) indicated that Well I had a sand net thickness of about 328 ft (100 m) in Nukhul formation. However, the well was completed with total perforation intervals of 150 ft (46 m) in 5′ liner.

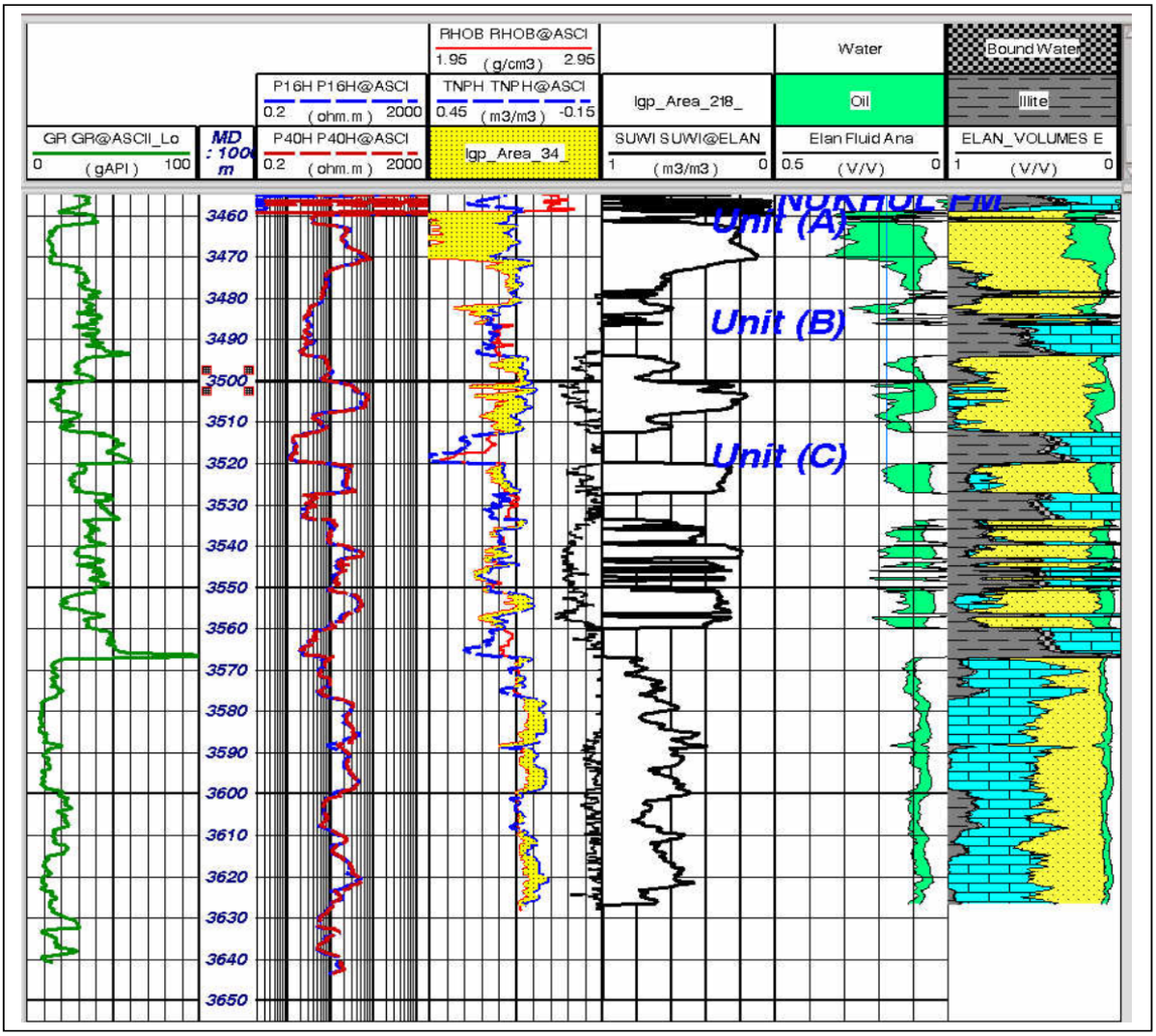

FIG. 3 WELL LOGS OF WELL I

TABLE 2 PRODUCTIVITY INDEX OF NUKHUL FORMATION IN WELL I

No	Interval	layer	h_{perf}	$h_{net\ perf}$	$h_{vertical}$	$h_{vertical}$	Ø	$K_{Correlation}$	Kh	P.I.	Completion factor	P.I.cor
	Meter		Meter	Meter	Meter	ft	%	md	md.ft	bpd/psi	Fraction	bpd/psi
1	3462-3472	A	9	9	4.5	14.8	14.5	97.5	1440	0.441	0.25	0.110
2	3494-3498	B	14	4	2	6.6	16	217.0	1424	0.436	0.25	0.109
3	3498-3501			3	1.5	4.9	10	34.0	167	0.051	0.25	0.013
4	3501-3508			7	3.5	11.5	17	295.6	3394	1.039	0.25	0.260
5	3520-3525	C	7	4	2	6.6	19	548.4	3598	1.101	0.25	0.275
6	3525-3527			2	1	3.3	16	217.0	712	0.218	0.25	0.054
7	3540-3544	C	8	3	1.5	4.9	19	548.4	2699	0.826	0.25	0.207
8	3544-3548			1.5	0.75	2.5	21	1017.4	2503	0.766	0.25	0.192
9	3552-3555	C	8	3	1.5	4.9	14	117.0	576	0.176	0.25	0.044
10	3555-3560			3	1.5	4.9	18.5	469.9	2312	0.708	0.25	0.177
Total			46	39.5	19.8	64.80				5.8		1.4

h_{perf} : Gross perforated thickness (measured thickness)

$h_{net\ perf}$: Net perforated thickness (measured thickness)

$h_{vertical}$: Net perforated thickness (vertical thickness – well inclination is about 60°)

Ø : Formation porosity from the logging

$K_{Correlation}$: Formation permeability (obtained from the porosity/permeability plot of the formation)

P.I. : Productivity index

Completion Factor : It is a correction factor to adjust the calculated P.I. It considers the effect of the completion in the productivity of the formation. It is estimated from the actual data of the offset wells in the same formation.

$P.I._{cor}$: Corrected productivity index

The productivity index of Nukhul formation in Well I was theoretically calculated as shown in Table 2. It was found that the estimated productivity index was about 1.4 bpd/psi which was too close to the average productivity index of Nukhul formation in the offset wells. However, the analysis of the vacuum test (which was performed during the completion of the well) showed that the well productivity index was only about 0.5 bpd/psi. This may be attributed to the presence of formation damage in the area around the wellbore due to the mud losses during the drilling operations of Well I. Accordingly, after review the wells history in the same area, the decision was taken to perform acid stimulation job to remove the formation damage due to the mud losses.

Table 3 presents the core experiment analysis of Nukhul formation. This table demonstrates the possibility for acidizing of Nukhul formation.

Nukhul formation is mostly sandstone rock with cementing material of dolomite mineralogy which would react with treating acid favoring in cleaning and regaining enhanced permeability for the formation. Therefore, the nitrified 15% HCl was selected as the main treating acidizing fluid. The nitrified acid was selected to work as diversion for the long perforation interval. This can get improvement by enlarging pore size.

The acidizing program was generated using empirical rules based on previous field experience in Nukhul formation. The acidizing program included injection of 8000 gal of the nitrified 15% HCl acid. The main additives were as follows:

- Acid corrosion inhibitors (2% - 160 gal): it is composed of polar organic compounds capable of adsorbing onto the metal surface, thereby establishing a protective film that acts as a barrier between the metal and the acid solution.Surfactants (0.5% - 40 gal): it was used to break undesirable emulsions, reduce surface and/or interfacial tension, and speed clean up.

TABLE 3 CORE EXPERIMENT ANALYSIS OF NUKHUL FORMATION

Potential formation damage of mineral components				
Sensitive mineral	**Potential problem**	**Avoid using**	**Use**	**Treatment to eliminate problems**
Carbonates	Calcium-fluoride and iron-hydroxide	HF acid, oxygen-rich systems	HCl or acetic acid, oxygen scavengers	Acidize with HCl and use suitable chelating agent.
Pyrite	Iron-hydroxide precipitate sulfate production	Oxygen-rich systems, fluid contain Ca+2, Sr+2, Ba+2	Acid systems, oxygen scavengers	Acidize with HCl/HF and use correct flushes
Kaolinite	Migration of fines	High flow rates and high transient pressures	Low flow rates and low transient pressures	Use a clay stabilizer
Silicates (clays and feldspars)	Silica	Concentrated HF	Dilute HF	Acidize with HCl/HF and use correct flushes
Mixed-Layer Illite/Smectite	Swelling/iron-hydroxide precipitate	Fresh-water system/oxygen -rich system, high pH	KCL or hydrocarbon system	Acidize with HCl/HF and use suitable chelating agent

Anti-sludge agent (1% - 80 gal): when acid contacts some crude oils, sludge can form at the acid/oil interface. As a result, the sludge accumulates in the formation and decreases the formation permeability. To combat the formation of sludge, cationic and anionic surfactants were used to adsorb and provide a continuous layer of protection at the acid/oil interface.

- Clay stabilizer (10 gal/Mgal – 80 gal): it was used to prevent the damage that may occur from the swelling of the clay.
- Mutual solvents (5% - 400 gal): it is chemical that is mutually soluble in both hydrocarbons and water. Mutual solvents were used to
  - ✓ aid in reducing water saturation around the wellbore by lowering the surface tension of the water to prevent water blocks
  - ✓ aid in providing a water-wet formation to maintain the best relative permeability to oil
  - ✓ help to prevent stabilizing emulsions
  - ✓ help to maintain the required concentration of surfactants and inhibitors in solution by reducing adsorption of these materials
  - ✓ dissolve any oil on the formation pore surface
  - ✓ serve as a de-emulsifier
- pH control (3% - 240 gal): it was used so that a low pH is maintained after the HCl is spent. A low pH aids in preventing the secondary precipitation of iron.
- Iron sequestering agents (50 lb/Mgal – 400 lb): these agents bond to the iron and hold it in solution so that it cannot precipitate.

The treatment fluid was displaced into the formation with 6500 gal of foamed sea water and surfactant. Surfactant helps to reduce the surface tension and capillary pressure of the fluid for better improved fluid recovery. This over-flush would displace the spent acid into the formation for improved results (Improve the clean-up of spent acid following treatment).

Fluid placement is critical to the success of the matrix stimulation treatment. In the acidizing job of Well I, a combination of employing coiled tubing and foam as diverting agents were used. Coiled tubing was used to spot the fluids along the zone, while reciprocating the tubing along the zone of interest.

To evaluate the acidizing job of Well I, vacuum test was performed after conducting the acidizing

program. Fig. 4 shows a comparison between the results of the vacuum tests before and after the acidizing job.

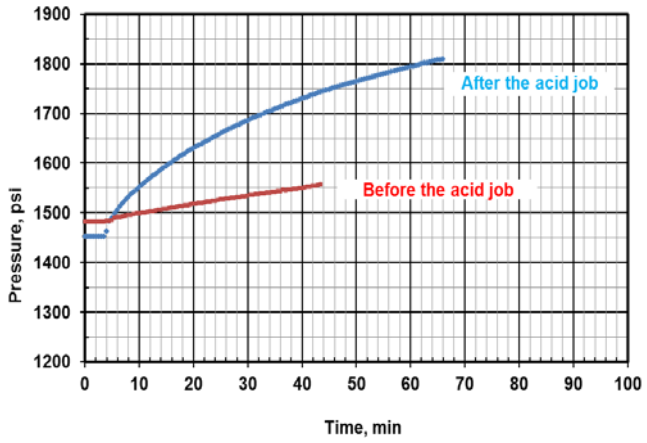

FIG. 4 VACUUM TESTS RESULTS BEFORE AND AFTER THE ACID JOB IN WELL I

It is clear from Fig. 4 that, after the acid job, the pressure intends to stabilize faster. This is an indicator for achieving better formation productivity and successful and effective acid job. The analysis of the vacuum test results showed that the well productivity increased from about 0.5 bpd/psi to 1.0 bpd/psi after the implementation of the acid job. When the well was put on production, the oil production rate was 560 bbl/day and water cut of 2%.

Conclusions

A comprehensive and cost-effective approach to diagnose and treat the formation damage problems is proposed. Application of such approach in oil producing well at Gulf of Suez area in Egypt achieved oil production rate of 560 bbl/day after complete mud loses during the drilling operations. The results of this case study was presented and analyzed.

REFERENCES

Ali, Y., "Development of an Advisor Auditor Computer Program for Acidizing Job Design." M.Sc. Thesis, Faculty of Engineering, Cairo University, 2011.

Allen, T.O., "Creative Task Force Attack on Profit Loss due to Formation Damage." Paper SPE 4658, presented at the SPE Annual Meeting, Las Vegas, Nevada, USA, September 30–October 3, 1973.

Beadie, G. "Well Productivity Awareness School (WPAS)." Paper SPE 30131, presented at the SPE European Formation Damage Conference, The Hague, Netherlands, May 15–16, 1995.

Brannon, D.H., Netters, C.K., and Grimmer, P.J., "Matrix Acidizing Design and Quality-Control Techniques Prove Successful in Main Pass Area Sandstone." Paper SPE 14827, Journal of Petroleum Technology, 931–942, August 1987.

Civan, F., "Reservoir Formation Damage: Fundamentals, Modeling, Assessment, and Mitigation." Second Edition, Gulf Publishing Company, Houston, Texas, 2000.

Hill, D.G., Liétard, O.M., Piot, B.M., and King, G.E., "Formation Damage: Origin, Diagnosis and Treatment Strategy." Reservoir Stimulation Book, Third Edition, Chapter 14, John Wiley & Sons, Ltd., 2000.

Smith, M.B., and Shlyapobersky, J.W., "Basics of Hydraulic Fracturing." Reservoir Stimulation Book, Third Edition, Chapter 5, John Wiley & Sons, Ltd., 2000.

Thomas, R.L., and Morgenthaler, L.N., "Introduction to Matrix Treatments." Reservoir Stimulation Book, Third Edition, Chapter 13, John Wiley & Sons, Ltd., 2000.

Wang, S., "Quickly Identifying Well Problem by Modern Production Analysis for a Better Stimulation Plan." Paper SPE 120639-MS, SPE Production and Operations Symposium, Oklahoma City, Oklahoma, 2009.

Mahmoud Abu El Ela is an associate professor at the Petroleum Engineering Department, Cairo University, Egypt, and works also as a project manager at WorleyParsons Engineers Egypt Ltd. Previously, he was a lead process engineer at WorleyParsons, assistant professor at the Petroleum Engineering Department at Cairo University, petroleum process consulting engineer for Khalda Petroleum Co., and a research engineer at Woodside Research Foundation (Curtin University of Technology, Australia). Since 1997, he has been a technical consultant in petroleum engineering for national and international companies. Abu El Ela holds a B.Sc. and M.Sc. in petroleum engineering from Cairo University, and a Ph.D. from Curtin University of Technology. He is a member of the Egyptian Engineers Syndicate and SPE.

Pervaporation Separation of Ethyl Butyrate/Wate Mixture: Experimental and Mass Transfer Investigation

Toraj Mohammadi*[1], Tavan Kikhavani[2]

Research Lab for Advanced Separation Processes, Department of Chemical Engineering, Iran University of Science and Technology, Iran

*[1]torajmohammadi@iust.ac.ir; [2]kikhavani@iust.ac.ir

Abstract

In this study pervaporation (PV) of ethyl butyrate (ETB)/water mixtures using synthesized poly (ether-block-amide) (PEBA) membranes was investigated. The membranes were made via solution casting on water surface (as non solvent). After studying the effects of different parameters on the membranes morphology, it was found that the mixture of (1 n-butanol/ 3 iso-propyl alcohol), temperature range from 70-800C and polymer concentration range from 4-7 wt could be used to obtain uniform membranes. PV separation of ETB/water mixtures was carried out using these membranes. The results showed that with increasing ETB concentration, both total permeation flux and ETB separation factor increase. Increasing temperature, in the studied limited range, resulted in decreasing separation factor and increasing permeation flux. With decreasing permeate pressure, permeation flux increased and separation factor decreased.

Overall mass transfer coefficient was evaluated using steady state ETB permeation flux equation. Membrane mass transfer coefficient, boundary layer thickness and liquid boundary layer mass transfer coefficient were calculated using the modified concentration polarization equation and the resistance in series model. Concentration polarization index (using membrane and liquid boundary layer mass transfer coefficients) was defined and used to present extent of the concentration polarization phenomenon.

The modified Arrhenius model was used to correlate ETB permeation flux and the operating temperature. Good agreement was observed between the experimental results and the model predictions. Results showed that the effect of temperature on sorption is greater than that on diffusion.

Keywords

ETB/Water Separation; Pervaporation; PEBA Membrane; Mass Transfer Coefficient; Concentration Polarization

Introduction

Membrane separation processes have been investigate d for long time in various applications. The rapid deve lopment of these processes is due to their environment al friendly properties, energy saving aspects, effective recovery and separation of volatile organic component s. They have different industrial applications such as f ood, chemical, petrochemical (CO2 capture and separa tions) and so on. Pervaporation (PV) process has a go od potential for separating liquid mixtures of volatile i ngredients. PV can be used for concentration or recove ry of organics from aqueous solutions (Li et al. 2008), s eparation of organic mixtures (Sridhar et al. 2004) and so on.

Aroma compounds in juice which are responsible for a typical juice flavor are very sensitive to heat, thus con ventional processes that involve evaporation may caus e loss of these compounds and change the juice flavors. Therefore, these aroma compounds should be recover ed with process such as PV, which can conserve them without any loss.

In this study, synthesized poly (ether-block-amide) (P EBA) membranes were used for recovery of ETB/water mixtures. The PEBA membranes were prepared via ca sting solution method. At first, the effects of different parameters, such as ratio of solvents, temperature and concentration of polymeric solution were investigated on membrane formation. After that, the prepared mem branes were evaluated in PV process. Finally, the over all, membrane and liquid boundary layer mass transfe r coefficients were calculated and the extent of concent ration polarization was predicted. Modified Arrhenius model was used to correlate ETB permeation flux and operate temperature and the effects of temperature on

separation mechanism (sorption and diffusion) were st udied in details.

Experimental

Materials

PEBA (as granule) was supplied by Atochem Company. n-Butanol (74.12 g/mol, 0.812 g/cm^3), isopropyl alcohol (60.1 g/mol, 0.786 g/cm^3, max. 0.005% H_2O) and ETB (for synthesis, 116.16 g/mol, 0.88 g/cm^3) were purchased from Merck Chemical Company. The microporous polysulfone (PS) membranes [ultrafiltration (UF) pHT20-6338] were used as support layer, provided by Dow Denmark, Inc. Physical and thermodynamic properties of ETB are given in Table 1.

TABLE 1 PHYSICAL AND THERMODYNAMIC PROPERTIES OF ETB (Seeaders 1998; Perry 1999; Lyman 1990)

Vapor pressure (pa)		2038
Infinite dilute diffusion coefficient (m2/s)		7.4×10^{-10}
Infinite dilute activity coefficient		1161
Henry law constant (pa/mol fraction)		2366118
Antoine constants	**A**	20.987
	B	3202.2
	C	56.6985

Membrane Preparation

PEBA membranes were prepared by casting the polymeric solution (PEBA + solvents) on the non-solvent (water) surface. Due to the solvent and non-solvent exchange, thin PEBA films were formed on the non-solvent surface. The PEBA membranes were put on the UF membranes (as support layers) for providing their mechanical strength. The details of membrane preparation and mechanism of membrane formation were described in our previous work (Mohammadi et al. 2008).

PV Setup and Expriments

PV apparatus used for PV experiments is presented in Fig.1. The upstream pressure was maintained at atmospheric pressure (using air release valve) and the downstream pressure was kept low with a vacuum pump. The amount of feed temperature and downstream pressure were recorded by thermostate and monometer, respectively. Permeation fluxes collected over a given period of time in a cold trap were weighed using a digital balance (PRECISA M310) with an accuracy of about 0.001 gr and analyzed using gas chromatography (GC-2010 Shimadzu).

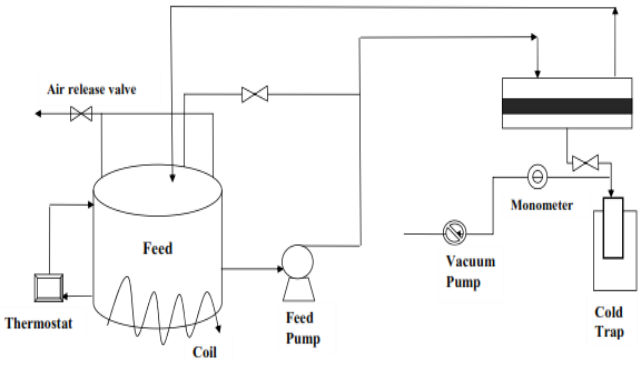

FIG. 1 SCHEME OF THE LABORATORY SCALE PV SETUP

Results and Disccution

Membrane Formation

After dripping the polymeric solution on the water sur face, because of the difference between polymeric solu tion and water surface tension, the polymeric solution was spontaneously spread on the water surface, and af ter the mutual diffusion of solution and non-solvent th e thin membrane film was obtained. The influences of different parameters such as ratio of solvents, polymer ic solution concentration and temperature on membra ne formation were investigated. The SEM photographs of PEBA membranes that synthesized at different solv ents ratio are shown in Fig. 2. As it can be observed th at ddition of iso- propanol improves the surface qualit y. With 1n- Butanol / 3 iso-propanol ratio, (Fig. (2.D)), t he defect-free membranes can be obtained and high se paration performance can be achieved. High quality fil ms were obtained in a (3/1) ratio of iso-propanol / n- B utanol, temperature range from 60-80^{0}C and polymer c oncentration range from 4-7 wt%. The effects of differe nt parameters on the membrane formation were descri bed in details in our previous work (Mohammadi et al. 2008).

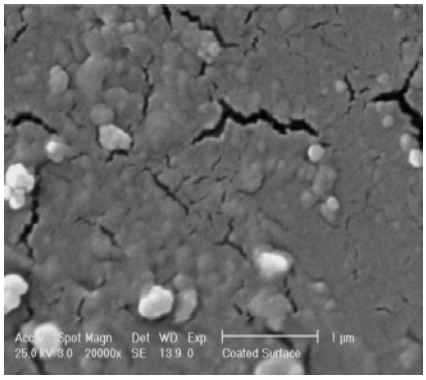

(A)

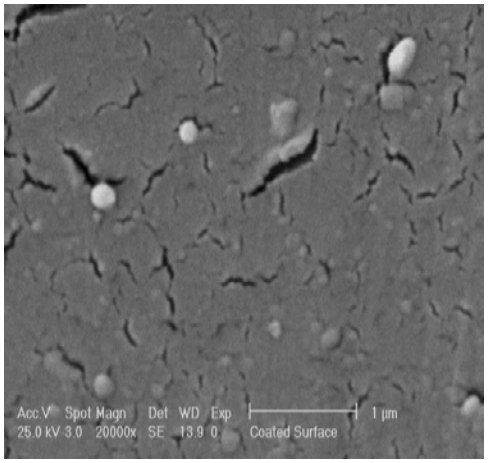

(B)

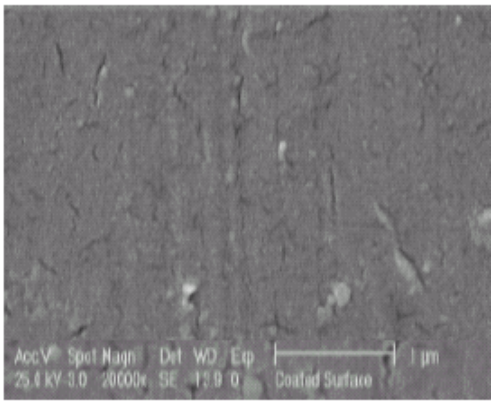

(C)

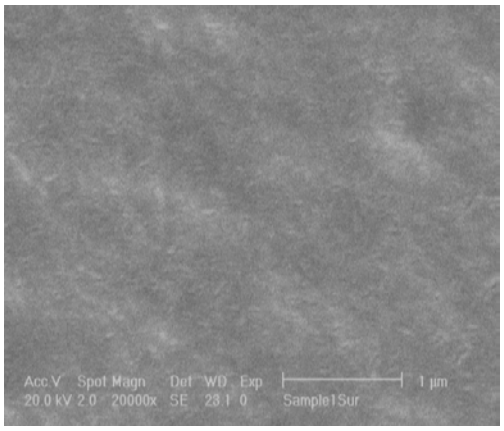

(D)

FIG. 2 SEM PHOTOGRAPHS OF THE MEMBRANES USING DIFFERENT SOLVENT RATIOS AT 75^{0}C
A: N- BUTANOL, B: 3 N-BUTANOL / 1 ISO-PROPANOL, C: 1 N-BUTANOL / 1 ISO-PROPANOL, D: 1N-BUTANOL / 3 ISO-PROPANOL

PV Experiments

PV experiments were carried out to separate ETB/water mixtures. The effects of feed concentration on permeation flux and separation factor is shown in Fig. 3. As observed, total permeation flux and ETB separation factor increase with increasing feed concentration. This can be described with enhancement of the liquid activity and the driving force for ETB transport. The effect of temperature on total permeation flux and ETB separation factor is shown in Fig. 4. With increasing temperature, total permeation flux increases but ETB separation factor decreases. Mobility of the polymer chains increases with increasing temperature, therefore the permeation flux of both ETB and water increase. Thus, ETB separation factor (the ratio of two permeation fluxes) decreases. The effect of permeate pressure on ETB permeation flux and separation factor is shown in Fig. 5. With decreasing permeate pressure, ETB permeation flux slightly increases, while ETB separation factor decreases. ETB is the organic compound with the high Henry's law constant. With decreasing the permeate pressure, ETB permeation flux increases slower than water permeation flux. Since low vacuum pressure is costly and also has negligible effect on ETB PV separation performance, in addition for recovery of ETB (with high saturated vapor pressure and high activity coefficient), a relatively high vacuum pressure is preferred (Hwang and She 2004).

Investigatin of Mass Transfer Phenomenon

PV can be classified into three categories, i.e. vacuum driven; temperature-gradient driven and carrier gas driven, although the common process is vacuum pressure driving force. In PV system, the molecular sizes of feed components are not so different that separation can be carried out based on molecular sieving. Therefore, porous membranes cannot be used and dense membranes are more applicable. As a result, separation occurs via solution-diffusion mechanism. This mechanism consists of sorption, diffusion and desorption steps (Jirarat ananon et al. 2002). PV has two potential sources of selectivity. The first one is the difference between permeabilities across the membrane which means one component in the feed mixture is more soluble or diffuses more rapidly through the membrane. The second one, such as one-stage distillation, is the relative volatility of one component in the liquid mixture. Therefore selectivity can be written as bellow (Cussler 2007):

$$\alpha = \left[\frac{D_1 H_1}{D_2 H_2}\right]\left[\frac{H_1'}{H_2'}\right] \quad (1)$$

Where, α, D, H, H' are selectivity, diffusion coefficient, Henry law constant and partition factor, respectively. The first and the second parts in Equation 1 come from the first (difference between permeabilities across the membrane) and the second (relative volatility of one

component in the liquid mixture) potential sources of PV, respectively.

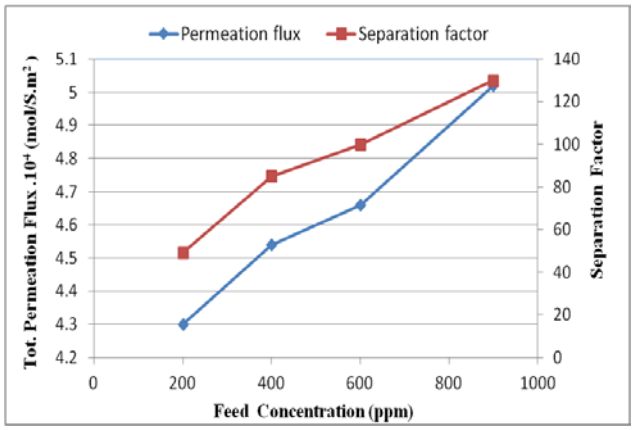

FIG. 3 EFFECT OF FEED CONCENTRATION ON TOTAL PERMEATION FLUX AND SEPARATION FACTOR AT 25°C

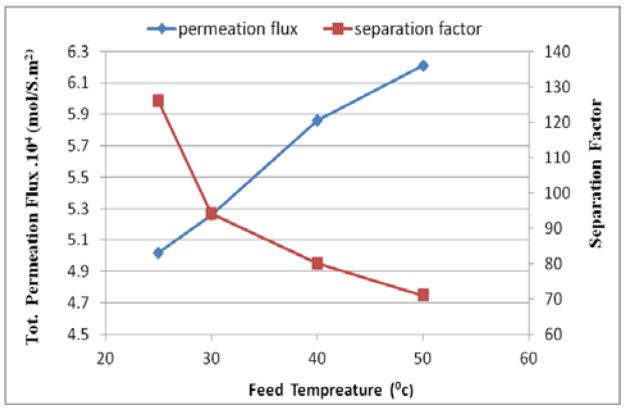

FIG. 4 EFFECT OF FEED TEMPREATURE ON TOTAL PERMEATION FLUX AND SEPARATION FACTOR 900 PPM

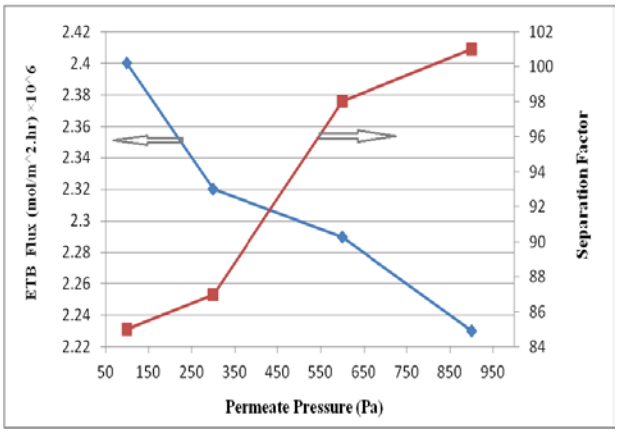

FIG. 5 EFFECT OF PERMEATE PERESSURE ON ETB PERMEATION FLUX AND SEPARATION FACTOR AT 400 PPM

Total permeation flux is the sum of ETB and water flux across the membrane:

$$J_t = J_w + J_E$$
$$J_E = J_t.y_E \qquad (2)$$
$$J_w = J_t.y_w$$

Where, J_t, J_E, J_W, y_E, y_w are total permeation flux, ETB pe rmeation flux, water permeation flux, ETB mole fractio n and water mole fraction in gas phase, respectively. F or a dilute solution, if the organic concentration in the permeate side is still low, separation factor can be writ ten as bellow:

$$\alpha = [\frac{y_E}{y_w}]/[\frac{x_E}{x_w}] \cong \frac{y_E}{x_E} \cong \frac{C_{EP}}{C_{Ef}} \qquad (3)$$

Where, x_E, x_w are ETB and water mole fraction in feed and C_{Ef}, C_{EP} are ETB concentrations in the feed and per meate side, respectively. The ETB and water fluxes can be written based on the non-equilibrium thermodyna mic equations. For this binary system (ETB and water), fluxes can be calculated by the following equations (H wang and She 2004; Jiraratananon et al. 2002):

$$J_E = \frac{Q_E P_E^{sat}}{l}(x_E\gamma_E^{\infty} - \frac{P_E}{P_E^{sat}}) = \frac{Q_E}{l}(x_E\gamma_E^{\infty}P_E^{sat} - P_E) \qquad (4)$$

$$J_w = \frac{Q_w P_w^{sat}}{l}(x_w - \frac{P_w}{P_w^{sat}}) = \frac{Q_w}{l}(P_w^{sat} - P_w) \qquad (5)$$

Where, Q, Psat and l are overall permeability, saturated vapor pressure and membrane thickness, respectively. (xEYEPEsat – PE) and (PWsat –PW) are driving forces for ETB and water transfer through the membrane, respectively. Furthermore, ETB flux can be described by mass transfer coefficients as follows (Hwang and She 2006):

$$J_E = K_E(C_{Ef} - \frac{PC_{Ep}}{H_E}) = k_{El}(C_{Ef} - C_{Em}) = k_{Em}(C_{Em} - \frac{PC_{Ep}}{H_E}) = C_{EP}.q \qquad (6)$$

Where, K_E, K_{El}, K_{Em}, C_{Em} and q are ETB Overall mass transfer coefficient, ETB mass transfer coefficient in liquid boundary layer, ETB mass transfer coefficient in the membrane active layer, ETB concentration within the membrane and total volume flux, respectively.

Overall mass transfer coefficient can be estimated by plotting ETB permeation flux against $(C_{Ef} – (PC_{Ep}/H_E))$. Since ETB has high Henry's law constant, permeation flux can be plotted verse C_{Ef}. Permeability can be related to overall mass transfer coefficient by the following equation(Hwang and She 2006):

$$Q_E = \frac{K_E.C_{tot}.lP_w^{sat}}{H_E} \qquad (7)$$

In dilute *PV*, C_{tot} (total molar volume concentration of f eed) is approximately equal to water molar volume de nsity (mol/m^3). Since ETB has high Henry's law constan

t, permeate pressure has negligible effect on permeatio n flux (Equation 7). Therefore, for calculation of memb rane permeability and overall mass transfer coefficien t, ETB permeation flux can be plotted verse ETB mole f raction in the feed. The membrane permeability was ca lculated from the slope of regration line in Fig. 6. The r esults showed that the membrane permeability is abou t 2.36 × 10-8 (mol/m2.s.Pa). Using Equation 7, the overa ll mass transfer coefficient is also about 1.018 × 10-6 (m /s).

According to resistance in series model, there are three resistances against mass transfer in the membrane process: feed, membrane and permeate resistances (Fig. 7a):

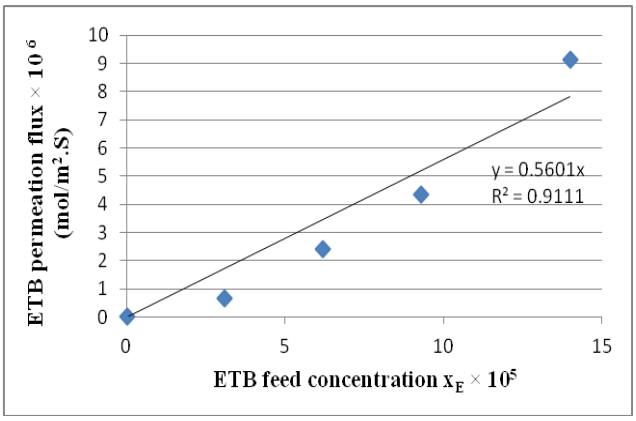

FIG. 6 ETB PERMEATION FLUX AS A FUNCTION OF FEED CONCENTRATION

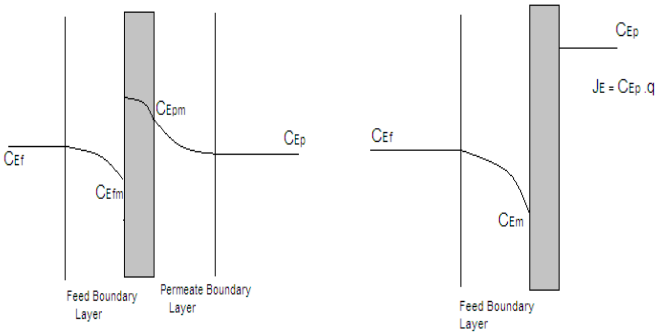

(a) (b)

FIG. 7 SCHEM OF THE MEMBRANE MASS TRANSFERETB

$$\frac{1}{K_E}=\frac{1}{k_{El}}+\frac{1}{k_{Em}}+\frac{1}{k_{Eg}} \quad (8)$$

Where, K_{Eg} is the ETB mass transfer coefficient in permeate boundary layer. In PV of a dilute ETB aqueous mixture using synthesized PEBA membrane, the support layer and the permeate side resistances are negligible. The scheme of mass transfer in this case can be presented according to Fig. 7b. Therefore, Equation 8 can be written as:

$$\frac{1}{K_E}=\frac{1}{k_{El}}+\frac{1}{k_{Em}} \quad (9)$$

The modified concentration polarization equation can be used for calculation of the membrane mass transfer coefficient and the boundary layer thickness. The simplified equation, for the non-ideal feed and high Henry's law constant,ca n be presented by the following equation (Hwang and She 2004):

$$Ln\left(\frac{1-C_{Ef}/C_{Ep}}{1-q/k_{Em}}\right)=-\left(\frac{\delta}{D_E}\right)q \quad (10)$$

Where, δ is the boundary layer thickness. The two unknown parameters (δ, k_{Em}) can be evaluated by the best fit method of the experimental data. The value of k_{Em} was initially estimated based on K_E and linear regression was used to calculate δ. The final value of k_{Em} was adjusted by the optimum value of the linear regression standard, R^2 (Hwang and She 2004).

The effect of permeate pressure on the membrane performance can be investigated by the following equation(Hwang and She 2004):

$$\frac{1}{\alpha}=\frac{1}{Q_r H_r}+\left(\frac{Q_r-1}{Q_r H_r}\right)P_r \quad (11)$$

$$Q_r=\left(\frac{Q_E}{Q_w}\right) \quad (12)$$

$$H_r=\left(\frac{P_E^{sat}\gamma_E^{\infty}}{P_w^{sat}}\right) \quad (13)$$

$$P_r=\left(\frac{P}{P_w^{sat}}\right) \quad (14)$$

The reciprocal of separation factor *(1/α)* verse relative pressure *(P_r)* is shown in Fig. 8. The relative membrane permeability *(Q_r)* and the relative Henry's law constan t *(H_r)* were obtained by using slope and intercept of th e plot. As calculated, Q_r is less than 1. which means tha t with decreasing permeate pressure ETB permeation f lux increases with lower rate than water permeation fl ux (because of the higher ETB Henry's law constant).

The best-fit method using Equation 10 was used for cal culation of the membrane mass transfer coefficient and the boundary layer thickness. Linear regression analy sis for PV separation of ETB is shown in Fig. 9. The bo undary layer thicknesses were calculated from the slo pe of the regression line. As calculated, the membrane mass transfer coefficient and the boundary layer thick ness are 9.89 × 10^{-5} *(m/s)* and 7.4 × 10^{-4} *(m)*, respectively. The boundary layer mass transfer coefficient is also 1. 02 × 10^{-6} *(m/s)* (as calculated using Equation 9).

The polarization index was also used to evaluate the c oncentration polarization phenomena. This parameter has numerical range from 0 to 1 and can be calculated using the following equation (Hwang and She 2006):

$$I = \frac{k_{El}}{k_{Em} + k_{El}} \quad (15)$$

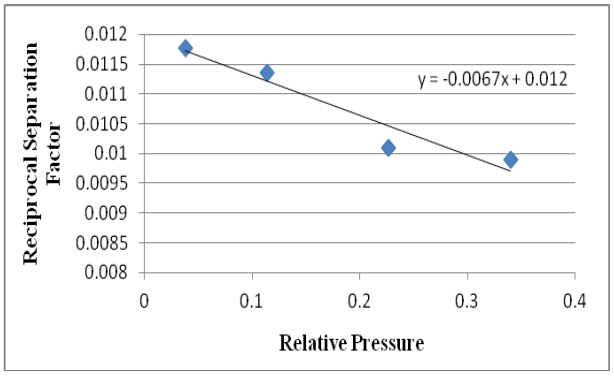

FIG. 8 RECIPROCAL SEPARATION FACTOR AS A FUNCTION O F RELATIVE PRESSURE

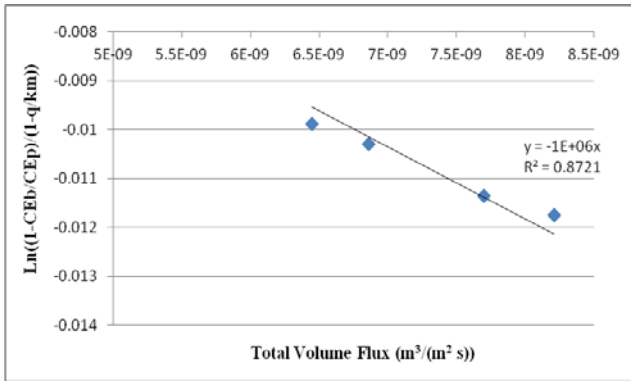

FIG. 9 LINEAR REGRESSION ANALYSIS FOR PV SEPARATION OF ETB

When, $I \approx 0$ and $I \approx 1$ concentration polarization is serious and neglectable, respectively. Using the mass transfer coefficients, the polarization index was calculated to be 0.01. This means that the concentration polarization is serious.

Modified Arrhenis Model

The relationship between permeation flux and feed temperature can be presented using the Arrhenius type formula [11]:

$$J_E = A' \exp(\frac{-E_{EP}}{RT}) \quad (16)$$

Where, A', EEP, T and R are correlation factor, PV activation energy, temperature and gas constant, respectively.

Another relationship between feed temperature and permeation flux can be described using activation energy of the vapor pressure (EEv) and activation energy of membrane permeability (EEm) (Hwang and She 2006):

$$LnJ_E = LnJ_{E0} - \frac{E_{Ev}}{R(T-C)} - \frac{E_{Em}}{RT} \quad (17)$$

$$LnJ_{E0} = \frac{\gamma_E^{\infty} x_E}{l} \exp(A + A_m) \quad (18)$$

Where, A' is correlation coefficient and A, B and C A, B, C are Antoine's constants.

EEv is positive and can be derived from the Antoine's equation (Hwang and She 2006):

$$LnP_E^{sat} = A - \frac{B}{T-C} = A - \frac{E_{Ev}}{R(T-C)} \quad (19)$$

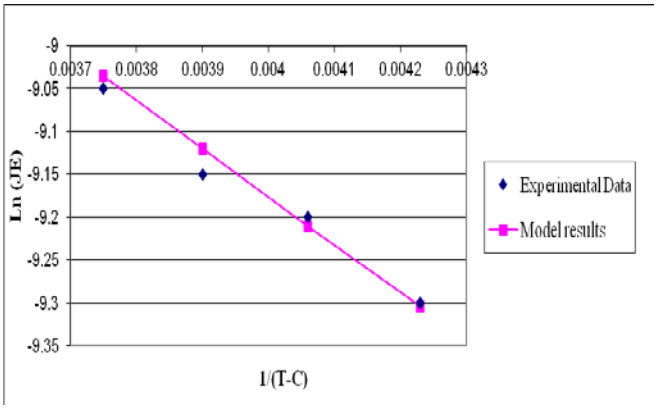

FIG. 10 MODIFIED ARHENIUS RELATIONSHIP FOR ETB AT FEED CONCENTRATION OF 900 PPM

However, Eim can be positive, negative or zero and can be obtained from the Arrhenius type relationship(Hwang and She 2006):

$$LnQ_E = A_m - \frac{E_{Em}}{RT} \quad (20)$$

EEv can be calculated using Equation 18 and EEm can be obtained by correlating overall permeabilities with temperature (Equation 20). Equation 16 can be used to predict the model results.

The modified Arrhenius relationship can explain the effect of feed temperature on permeation flux.

The activation energy of vapor pressure for ETB and water are 26600 and 143900 J/mol.K, respectively. E_{Em} was obtained as -33262.6 J/mol.K for ETB. The experimental data and the model predictions are illustrated in Fig. 10. The experimental results and the model prediction values show good agreement and consistency.

Increasing feed temperature affects both sorption and diffusion. Diffusion coefficient increases with increasing temperature. On the other hand, ETB

solubility decreases with temperature because of the exothermic sorption process. Therefore, the extent of the temperature effect on sorption or diffusion determines the sign of the activation energy of membrane permeability. Increasing temperature increases ETB permeation flux due to increasing its driving force by affecting its vapor pressure. Therefore, the negative values of E_{Em} for ETB and water mean that the effect of temperature on sorption is greater than that the on diffusion.

Conclusions

In this research, synthesis, characterization and performance of poly (ether block amide) membranes were studied. High quality membranes were obtained using a (3/1) ratio of iso- propanol / n-butanol, temperature range from 70-80 ^{0}C and polymer concentration range from 4-7 wt%. High performance was achieved for recovery of ETB from water with the PEBA membranes. It was observed that permeation flux and separation factor increase by increasing the ETB concentration in the feed. By increasing temperature and decreasing permeate pressure, permeation flux rises enhance but membrane selectivity diminishes. With decreasing permeate pressure, ETB permeation flux increase with lower rate than water permeation flux. Thus, ETB separation factor decreases by decreasing permeate pressure.

Mass transfer coefficients and boundary layer thickness were also calculated. It was found out that concentration polarization is almost serious.

Modified Arrhenius model was used to correlate ETB permeation flux and operate temperature. The results showed that the effect of temperature on sorption is greater than that on diffusion.

REFERENCES

Cussler, E. L. "Diffusion Mass Transfer in Fluid Systems." third edition, University of Minnesota, Cambridge University Press, New York, 2007.

Hwang, S. T. , and She, M. "Effects of concentration, temperature, and coupling on pervaporation of dilute flavor organics." Journal of Membrane Science 271 (2006): 16–28.

Hwang, S. T., and She, M. "Concentration of diluteflavor compounds by pervaporation: permeate pressure effect and boundary layer resistance modelling." Journal of Membrane Science 236 (2004): 193–202.

Jiraratananon, R., Sampranpiboon, P., Uttapap, D., Feng, X., and Huang, R.Y.M. "Pervaporation separation of ethyl butyrate and isopropanol with polyether block amide (PEBA) membranes." Journal of Membrane Science 173 (2000): 53–59.

Jiraratananon, R., Chanachai, A., and Huang, R.Y.M. "Pervaporation dehydration of ethanol-water mixtures with chitosan/hydroxyethylcellulose (CS/HEC)composite membranes II. Analysis of mass transport." Journal of Membrane Science 199 (2002): 211–222.

Li, L., Luo, Y., Tan, Sh., Wang, H., Wu, F., Liu, X., and Zhang, Z. "PPMS composite membranes for the concentration of organics from aqueous solutions by pervaporation." Chemical Engineering Journal 137 (2008): 496-502.

Lyman, W. J., Reehl, W. F., Rosenblatt, G. H. "Handbook of Chemical Property Estimation Methods." American Chemical Society, Washington DC, 1990.

Mohammadi, T., Kikhavani, T., and Moghbeli, M. "Synthesis and Characterization of Poly(ethe block-amide) Membranes for Organic/Aqueous Mixtures." Journal of Applied Polymer Science 107 (2008): 1917-1923.

Perry, R. H., "Chemical Engineer's Handbook", edited by Robert Perry, Mc Graw- Hill companies, 1999.

Seaders, J. D. "Separation processes principles." John Wiley & sons publishing co., 1998.

Sridhar, S., Smitha, B., Suhanya, D., and Ramakrishna, M. "Separation of organic–organic mixtures by pervaporation—a review." Journal of Membrane Science 241 (2004): 1-21.

Toraj Mohammadi Born in Iran in 1965, graduated as BSc from Abadan Institute of Technology, as MSc from Tehran Universiy and as PhD from UNSW in 1995. He has been employed as Professor of Chemical Engineering in Iran University of Science and Technology, in addition, he has published more than 200 ISI papers, and supervised more than 150 MSc and 10 PhD students.

Tavan Kikhavani recived her bsc in chemical engineering from tehran university (2003) and her msc from iust (2006). she has some publications in the area of membrane synthesis and is currently doing her phd at iust in the field of membrane separation processes.

Nomenclature

A	Antoine's constant
*A*m	correlation coefficient in Arrrhenius equation
B	Atoine's constant
C	Antoine's constant
C_{Ef}	ETB concentrations in the feed solution (mol/m^3)
C_{Ep}	ETB concentrations in the permeate (mol/m^3)
C_{Em}	ETB concentration within the membrane (mol/m^3)
D	Diffusion coefficient in aqueous solution (m^2/s)
E_{Em}	activation energy of membrane permeability for ETB (J/mol)
E_{EV}	activation energy of vapor pressure for ETB (J/mol)
E_P	the activation energy of PV
H′	Partition coefficient
H	Henry's law constant
H_r	Relative Henry 's law
J	Permeation flux
K_E	ETB Overall mass transfer coefficient (m/s)
k_{EL}	ETB mass transfer coefficient in liquid boundary layer (m/s)
k_{Em}	ETB mass transfer coefficient in membrane active layer (m/s)
k_{Eg}	ETB mass transfer coefficient in permeate layer (m/s)
l	membrane thickness
P	total permeate pressure (Pa)
P_E	partial permeate pressure of ETB (Pa)
P_w	partial permeate pressure of water (Pa)
P_{sat}	saturated vapor pressure (Pa)
P_r	Relative pressure
T	Temperature
Q	Overall permeability (mol/(m s Pa))
Q_r	Relative permeability
q	Total volume flux (m^3/(m^2 s))
R	Gas law constant
x	Mole fraction in liquid phase
y	Mole fraction in gas phase
Greek letters	
α	Separation factor
γ^{∞}	Activity coefficient in infinitely dilute aqueous solution
δ	Boundary layer thickness (m)
Subscripts	
E	ETB
W	Water
t	Total
f	Feed stream
m	membrane
P	permeate
l	Liquid boundary layer

Acquisition, Processing and Evaluation of Down Hole Data for Monitoring Efficiency of Drilling Processes

Maurizio Bevilacqua[1], Filippo Emanuele Ciarapica[1], Barbara Marchetti[2]

[1] DIISM-Università Politecnica delle Marche,Via Brecce Bianche 12, 60131, Ancona, Italy

[2] Università degli Studi eCampus, Via Isimbardi 10, 22060, Novedrate (CO), Italy

[1]m.bevilacqua@univpm.it; [1]f.ciarapica@univpm.it; [2] barbara.marchetti@uniecampus.it

Abstract

This paper presents a study carried out in collaboration with a company leader in the production of drilling tools and sensors. Data were gathered during a period of four months in two horizontal well of an oil field with the aim of assessing the relationship between Mechanical Specific Energy (MSE) and drilling efficiency trough the analysis of the most significant drilling parameters.

There are several models and measurement systems available for measuring such parameters, however in many practical cases the possible maximum performances are not achieved and this suggests the idea that there is still room, from a research point of view, to increase acquisition accuracy and their correct evaluation. In this study, down hole data were acquired to calculate significant parameters for assessing drilling performances which can contribute to the avoidance of errors in torque calculation due to the effect of drill string friction and the consequent distortion of MSE curve.

Moreover, the same data implemented in a model for Rate of Penetration (ROP) calculation and a map correlating RPM and Weight on Bit (WOB) values with Rate of Penetration was drawn.

Keywords

Mechanical Specific Energy; Drilling Rate; Weight on Bit; Drilloff Curve

Introduction

Oil well drilling, a complex and difficult control process, is characterized with low efficiency.

Nowadays the oil well costs are very high and the optimization of the process, in terms of increasing performances and reducing time, is a key factor for success. Systems for monitoring in real time parameters affecting drilling processes have been gaining increasing importance. Today's sophisticated data acquisition systems for both surface and downhole drilling data have greatly enhanced the understanding of the basic drilling mechanics and helped in the identification of major dysfunctions particularly harmful downhole vibrations. Various methods are now being used to optimize drilling practices by monitoring efficiency indicators such as mechanical specific energy and preventing harmful vibrations by adjusting drilling parameters in real time (Pessier and Fear M.J., 1992). In this study data acquired on field have been analyzed to evaluate and identify issues of drilling processes Diagnostic tool has been used whose concept and relative formula were introduced in 1964 (Teale, 1965) MSE is defined as the amount of energy required per unit volume of rock drilled and represents the energy necessary to drill a fixed volume of rock (Kpsi).

The monitoring of MSE can provide information for recognizing dull or damaged bits; select an appropriate bit and WOB and RPM for a bit and rock type, respectively; and avoid the poor mud circulation.

Another important parameter that influences the drilling performances is the geology of the formation. In order to identify its main characteristics such as the resistance and abrasiveness of the rock and the best drilling strategy, there are different available techniques.

The most widespread measurements performed are:

- gamma ray emitted by the soil that is able to to estimate the presence of clay;
- compressive acoustic transit time that provides information on the rock porosity and consequently on the type of constituent material;
- mechanical resistance of the rock.

This last parameter can be evaluated in two ways: measuring the Unconfined Compressive Strength (UCS) and the Confined Compressive Strength (CCS). UCS represents the force, applied to a defined area A, necessary to deform the rock at atmospheric pressure; whose value is characteristic and fixed for each type of formation and represents the minimum value of the relative mechanical resistance. CCS is the force on a defined area A, needed for the deformation of a volume of rock around which is applied to a pressure P. CCS measures the maximum value of the resistance for each rock. The Real value of the Compressive Strength (RCS) of a defined formation will be an average value within UCS and CCS

The overall efficiency of the drilling process can be evaluated as: μ=RCS/MSE.

Its maximum value corresponds to the minimum energy introduced in the system, e.g to the value of UCS.

The monitoring of MSE represents a key element of the Fast Drill Process (FDP); a process that aims at drilling with the highest possible ROP (technically and economically). ROP is the measured distance that the drill bit or other drilling tool penetrates the subsurface formations in a unit length of time. All optimization schemes focus on identifying the best of these parameters relative to other settings.

MSE should be kept as low as possible and ROP as high as possible in order to increase the efficiency of the process; which can be obtained by varying WOB, rotary speed, and mud flow within normal operating limits. Other than identifying performances limiting factors, MSE can be used as a quantitative measure for assessing costs-benefits associated with redesign of drilling process.

Usually drilling engineers want to maintain MSE value as close as possible to a formation's true compressive strength. Unexpected changes in MSE may indicate changes either in rock properties, or drilling inefficiency, or both.

It has been demonstrated that MSE can be used to identify the three most common causes of inefficiencies: bit balling (due to the accumulation of drilled material on the cutting tool that causes the energy transferred to the rock formation to decrease), bottom hole balling (caused by the accumulation of material at the bottom hole that reduces the energy transfer from the bit to the rock below it), and vibrations.

In this study the acquisition of the field data has been performed in collaboration with a company leader in the production of drilling tools and sensors that, for privacy reasons, is not named. This paper is organized in the following manner: a brief scientific background; a description of the material and methods used; the results obtained and the tests performed, with some examples explaining their diagnostic value; discussions of the results and conclusions.

Scientific Background

There are several authors that have studied and developed tools and relationships for optimizing drilling performances as well as have investigated the correlation between Mechanical Specific Energy with drilling efficiency. One of the most common test for the optimization of the drilling performance is the "drill rate" test, in which various WOB and RPM settings are experimented. Weight on bit is the total amount of downward force placed on a bit by the entire weight of the drill stem. The drillers then use the combination of WOB, RPM and torque settings which provide the best rate of penetration.

The curve represented in figure 1, known as drilloff curve (Dupriest and Koederitz, 2005), identifies three main regions of bit efficiency: in regions I and III the bit operates in conditions of inefficiency where a disproportionate amount of energy has to be used for a given ROP; in region II, instead, the bit works at its maximum efficiency giving that an increase of WOB produces a linear increase of ROP and a consequent constant value for MSE. The point in which the rate of penetration stops responding linearly with increasing weight on bit is referred as the a founder point and it is characterized by the optimum value of WOB. A variation of the MSE value indicates that the system exits from the linear region and is foundering; in this way the real time monitoring of MSE allows the driller to verify if the system is above or below the founder point and how it reacts to the variation of defined parameters and to improve well control practices, bit selection, design of bottom hole assembly, directional target sizing and makeup torque.

It was demonstrated that the real time monitoring of MSE can reveal drilling inefficiencies and give indications on the time to pull worn Polycrystalline Diamond Compact (PDC) bits (Waughaman et al., 2002); MSE and bit-specific coefficient of sliding friction were used to quantify the most common drilling issues (Pessier et a., 2012). A tool that

incorporates specific energy evaluation to model bit performance and predicts the rate of penetration of different bit types was developed (Guerrero and Kull, 2007).

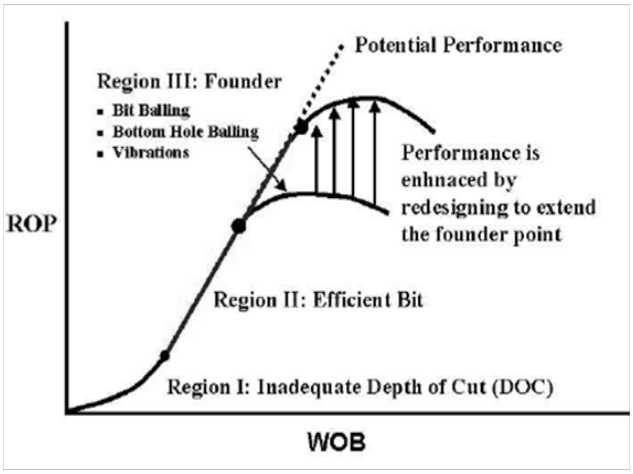

FIG. 1 DRILLOFF CURVE (DUPRIEST AND KOEDERITZ, 2005)

Experimental results demonstrated the importance of including bit hydraulics into the specific energy analysis for drilling optimization (Armenta, 2008). An attempt to better model downhole drilling was made by introducing the hydraulic energy term in the MSE correlation by means of defining it as Hydro Mechanical Specific Energy (HMSE); while experimental and field data showed that HMSE can identify inefficient drilling conditions (Mohan and Adil, 2009). The effects of changing the drilling parameters, bit wear and bit designs on ROP for both MSE and ROP model approaches were demonstrated and a commercial drilling simulator was used to model the rate of penetration sensitivities; these results were then compared to the results obtained using the MSE equation (including the bit hydraulic effects). They addressed benefits and disadvantages of using each method including their limitations and possible applications in different drilling scenarios, particularly in terms of bit runs, well simulations in real time, preplanning and post analysis (Rashidi et al., 2010). The concept of specific energy was used to develop an algorithm to estimate the technical limit of specific energy from wireline sonic, lithology and pressure data in order to represent the inherent drilling difficulty posed by the combination of rock properties, depths and pressures that make up a field's drilling environment, thereby facilitating comparisons of drilling performance from different fields that take account of varying rock drillability (Curry et al., 2005).

As demonstrated from previous studies, MSE is both a qualitative and quantitative measure that helps identify inefficiencies in the drilling process; moreover its measurement allows predicting power requirement (bit torque and rpm) for a particular bit type to drill a given ROP in a given rock type, and the ROP that a particular bit might be expected to achieve in a given rock type (Caicedo et al., 2005). In the same research work a bit-specific coefficient of sliding friction to express torque as a function of WOB and to compute specific input energy MSE in absence of down hole data has been introduced. A new method was developed to determine input variables for bit performances prediction based on the specific energy prediction and confined compressive strength; which have been integrated to provide new capabilities for rapid and accurate log-based determination of the expected achievable rate of penetration and operating parameters for all the bit types.

A new drilling rate equation that describes the effects of weight on bit, rotary speed and differential pressure on rate of penetration was introduced and the concept of founder points was revised developing a field procedure to determine how to measure the founder point at the rig. Application of this technique resulted in the maximum drilling rate possible with minimum bit wear (Robinson et al., 2001)

The monitoring of the drilling activity trough the acquisition of significant parameter (to anticipate and avoid occurrence of possible problems during well drilling) has been addressed as one of the main element in the architecture of the intelligent system that they elaborated for planning an efficient oil well drilling process (Morooka et al., 2001)

Evaluation of the Drilling Process Efficiency: Materials and Methods

The MSE surveillance process provides the ability to detect changes in the efficiency of the drilling system, more or less continuously (Dupriest and Koederitz, 2005). This has improved performance by allowing the optimum operating parameters to be identified easily, and providing the quantitative data needed to cost-justify design changes to extend the current limits of the system. MSE analysis has resulted in redesign in areas as diverse as well control practices, bit selection, Bottom-Hole Assembly (BHA) design, makeup torque, directional target sizing and motor differential ratings.

The formula introduced by Teale for calculating MSE assumes that in conditions of perfect efficiency, its value would equal rock compressive strength. However, the efficiency of bits at peak performance is in the order of 30-40%, in order to make MSE easy to use tool for driller Teale proposed a value adjusted to include a mechanical efficiency factor (Effm).

In this work the modified Dupriest's formula was used as expressed in equation 1.

$$MSE_{adj} = Eff_m\left(\frac{4WOB}{\pi D^2}+\frac{480*N*T}{D^2*ROP}\right) \quad (1)$$

The relative variables are defined in table 1.

TABLE 1 VARIABLES OF MSE FORMULA

Variable	Definition	Measurement unit (US)	Measurement unit (SI)
MSE	Mechanical specific energy	kpsi	ksi
WOB	Weight on bit	klbs	kdaN
D	Bit diameter	Inches	mm
N	Rotary speed	RPM	RPM
T	Rotary torque	Kft.lbs	kN.m
ROP	Rate of penetration	ft/hr	m/hr

To calculated parameters of interest data acquired from down hole have been used; and the largest source of error in the evaluation of the MSE is indeed represented by the fact that surface data contain torque created by friction between the pipe and the borehole, causing drill string friction and distorting the curve in a way that the bit appears to be consuming much more energy than that in reality.

In this work data have been gathered from an innovative and versatile data acquisition and diagnostic tool consisting in a downhole multiple-sensor that allowed the real time monitoring of the drilling process as well as downhole conditions and post-well analysis with a high level of accuracy.

As an example, the difference between the surface torque (S-Torque) and the down hole one (DH-Torque), measured by the sensors placed in the drilling tool is shown in figure 2. The torque generated by the bit depends on the applied WOB, the type of formation, the bit and the mud used, the friction losses and dynamical effects; while the comparison between the S-Torque and the DH-Torque allows evaluating the losses due to the friction amidst the tool and the hole walls.

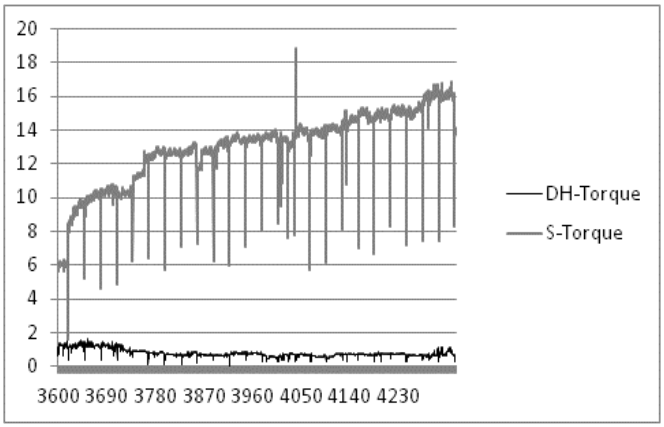

FIG. 2 DH-TORQUE VS S-TORQUE MEASURED IN WELL 1 DURING RUN 1

1) Measurement Tool

Beside WOB, ROP, Torque and relative MSE, there are other parameters of interest to evaluate, which can be measured by the tool containing different transducers:

- four extensimeter for the evaluation of bending moment, weight on bit and torque;
- two pressure transducers to measure internal and external pressure of the tool;
- four three-axial accelerometers for vibrations measurements;
- two magnetometers for evaluation of the rotational velocity;
- two thermocouples to measure downhole temperature.

Data are acquired and transmitted through a channel for each sensor with a frequency of 1 kHz.

The Bending Moment, generated by the gravity force acting on the drilling tool, by its contact with the hole walls, and by the curvature of the hole; is used to evaluate the curvature of the real trajectory and to compare it with the planned one. The internal and external pressure are influenced by the depth and geometry of the hole, the tool design, the loss of pressure at the bit, the flow rate and weight of the mud and ROP.

Moreover the tool is also able to monitor in real time the vibrations which allows increasing ROP, the components life and the hole quality.

All the vibrations involved in the drilling process are represented in figure 3.

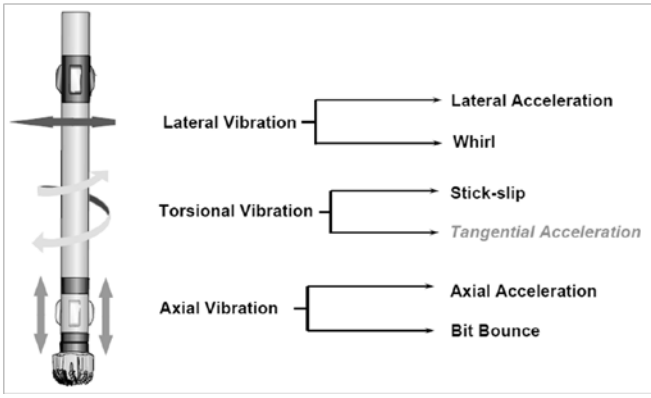

FIG. 3 TYPE OF VIBRATIONS IN THE DRILLING PROCESS

The lateral acceleration, induced by a movement perpendicular to the hole trajectory, if detected, requires immediate intervention to avoid damages to the equipments. The whirl consists in a eccentric rotation of the tool: in the forward whirl the tool rotates clockwise and causes the area of the collar that comes in contact with the hole to wear; in the backward whirl the center of the collar rotates around the center of the hole at an higher speed than expected, inducing the increase of the bending cycles and the consequent fatigue failure.

The major consequence of the whirl is a reduction of the efficiency and a larger hole diameter.

The stick-slip is a torsional vibration associated with a high torque and a fluctuation of RPM caused by the surface rotation of the drill string associated with its downhole deceleration due to the friction of the equipment with the hole walls. Also in this case it is requested an immediate intervention to avoid the ROP reduction and bit damages. Axial vibrations consist in the movement of the drill string along the hole axe; among which the most dangerous is the bit bounce.

For some of this parameters such as WOB, ROP, RPM and Torque the system visualizes the measured and processed values; for others, such as whirl and stick-slip, it provides a severity level (usually in a range from 0 to 7). Data are acquired against depth and time.

The main benefits introduced by this system are:

- real time monitoring and feedback of drilling process;
- early detection and resolution of drilling problems;
- optimization of the drilling process and relative safety issues;
- post drilling analysis and evaluation of bit performances.

Case Study: Monitoring of Drilling Parameters

In order to analyze the drilling parameters and optimize the process, the data have been acquired from two run performed in two different horizontal wells that pass through a limestone formation. Those wells have been chosen due to the homogeneity of the formation on almost all the length of the run.

All the data have been analyzed with the help of drilling engineers working for the company producing the measurement tools.

In the following Table, the main characteristics of the wells for each run are presented.

TABLE 2 WELLS CHARACTERISTICS

	WELL 1 Run 1	WELL 1 Run 2	WELL 2 Run 1	WELL 2 Run 2
Hole diameter (in)	6''	6''	6''	6''
In depth (m)	3571	4307	4865	5392
Out depth (m)	4307	4941	5392	5952
Drilling length (m)	736	634	527	560
Drilling time (h)	159.17	130	104.25	170
Bit type	PDC bit 9 blades, 8 mm cutters	PDC bit 9 blades, 9 mm cutters	PDC bit 9 blades, 8 mm cutters	PDC bit 7 blades, 11 mm cutters

1) Well 1, Run 1

In order to demonstrate the relationship between the drilling rate and performances and MSE, the following graphs present some of the main results obtained during the study.

In Figure 4, the graphs of MSEadj, ROP, WOB, RPM and Torque obt ained during the first run in well 1are presented.

In the graph of MSEadj a base-line has been drawn that separates the efficiency drilling zone from the foundering one. As an example one of this zone has been outlined, at about 4000 m of depth, which corresponds to a decreasing of ROP and an increasing of WOB and torque.

At the same depth the data show a decreasing of the tool inclination detected by the Near Bit Inclinometer (NBI), a variation of the bending

moment, the zeroing of the whirl and a spike of the pressure are shown in figure 5 a) and b).

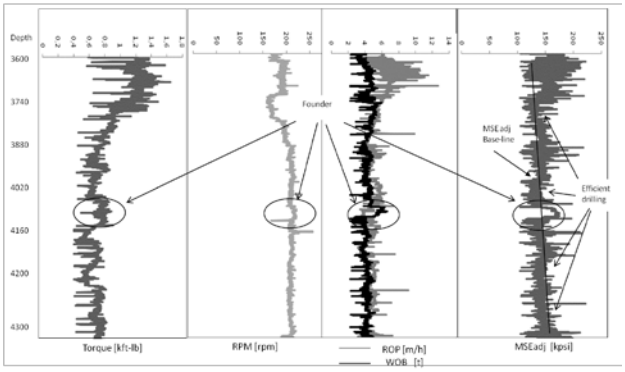

FIG. 5 A) FOUNDER POINTS IN WELL 1- RUN 1

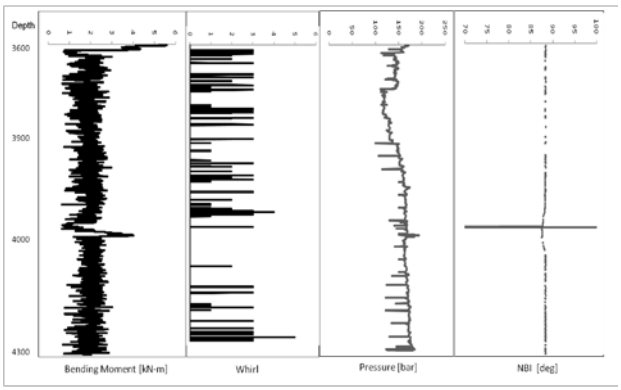

FIG. 5 B) FORMATION DEPENDENT PARAMETERS OF WELL 1- RUN 1

2) Well 1, Run 2

In order to assess the relationship between drilling rate and MSEadj values, a test was conducted during run 2 in well 1: WOB has been increased while observing the change of MSEadj. Results showed that if MSEadj remains close to its lowest value while increasing WOB, ROP increases linearly and the bit is operated in conditions of efficiency. Figure 6 shows the MSEadj and ROP values obtained during the test.

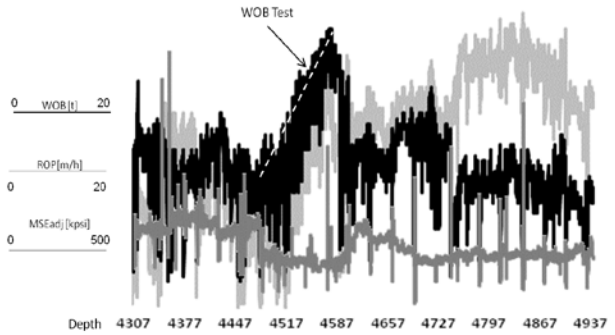

FIG. 6 WOB TEST CARRIED OUT IN WELL DURING RUN 2

Down hole data from run 2 of well 1, were implemented in the Bourgoyne and Young (1974), model to calculate ROP that is expressed as a function of several variables such as sediments compaction, pore pressure, bit weigh, rotary speed, impact force, bit hydraulics, bit wear.

The relative equation is composed of eight terms:

ROP= f1+ f2+ f3+ f4+ f5+ f6+ f7+ f8

Coefficients from a1 to a8 are experimental model constant and the other terms are described in table 3.

TABLE 3 TERMS OF ROP MODEL

f1	$e^{2.303a_1}$	Rock drillability effect (proportional with the rock strength of the formation)
f2	$e^{2.303a_2(10^3-D)}$	Depth effect (D = depth in feet)
f3	$e^{2.303a_3D^{0.69}(g_p-9)}$	Pore pressure effect; g = pore pressure in pounds per gallon equivalent
f4	$e^{2.303a_4D(g_p-P_C)}$	Overbalance on ROP effect; Pc = mudweight in pounds per gallon
f5	$[\frac{(\frac{w}{d_b})-(\frac{w}{d_b})_t}{4-(\frac{w}{d})_t}]^{a_5}$	Weight on bit effect; w = weight on bit; db = bit diameter
f6	$(\frac{N}{60})^{a_6}$	Rotary speed effect; N = revolution per minute
f7	e^{-a_7*h}	Bit wear effect; h= amount of bit wear
f8	$(\frac{F_j}{1000})^{a_8}$	Jet impact force effect; Fj= effect of bit hydraulic on ROP

The wear coefficient h was assumed equal to 5 x 10-8, data to calculate the ROP as function of RPM and WOB were measured on field and the model constants provided by the company.

In figure 7 the obtained ROP map in function of different combinations of RPM and WOB values applied to the PDC bit is presented. From the map it is evident that the highest ROP value is achieved in correspondence with high WOB values with low RPM. The lowest ROP value in the lower corner of the left-hand side indicates an inadequate depth of cut due to insufficient WOB and the lowest ROP value in the right-hand side of the map, identifies the combination of WOB and RPM that determine a incomplete depth of cut due to the fact that the bit has wear out completely.

3) Well 2, Run 1

During run 1 of well 2 at a depth of about 5200 meters, the rock strength increased approximately of 60% (passing from around 4 ksi to 7 ksi), with a consequent drop of the drilling rate. To address the ROP decrement, WOB was increased. The

monitoring of the MSEadj value, showed a quick increment from about 50 psi to 100 psi; which exceeded by far the influence of the change in rock strength, outlining the start of a vibrational founder due to a probable damage of the bit caused by the too high WOB value. This hypothesis was verified by rig personnel after pulling out the bit. In run 2 of well 2, at a depth of about 5900 meters, the hole passed through another formation with a similar same rock strength pattern (increasing of about 50%); and rig crews were instructed to reduce the WOB in order not to damage the bit. The monitoring of MSE trend indicated when the tool had fully penetrated the stringer, the drilling parameters could be set back at their original values.

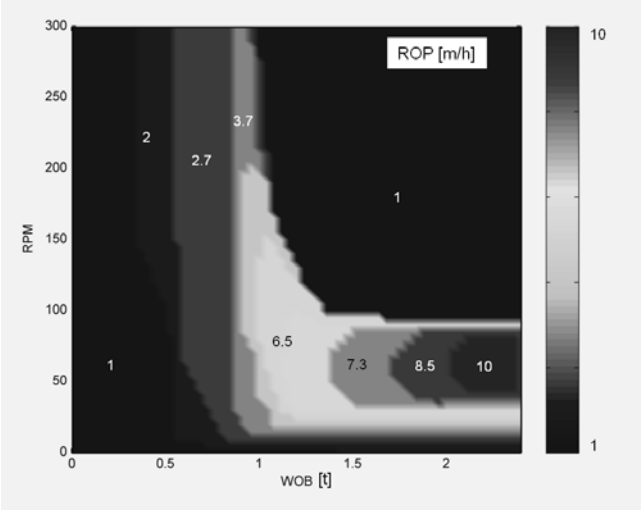

FIG. 7 ROP MAP

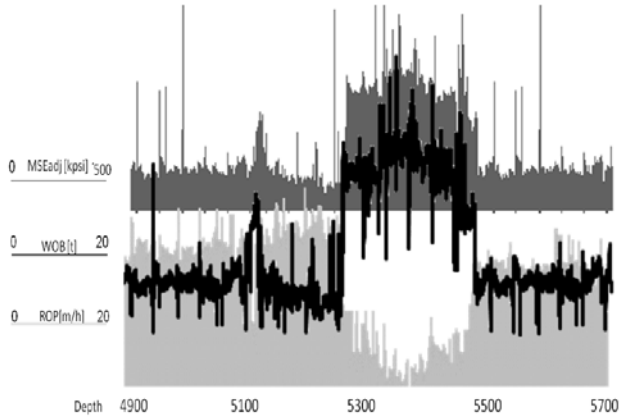

FIG. 8 VIBRATIONAL FOUNDER DUE TO BIT DAMAGE

Conclusions

In this work data from oil field well have been used to assess the main parameters affecting the drilling process. The results obtained showed how it is possible to use MSEadj having a monitoring tool to evaluate drilling efficiency.

In particular it has been demonstrated that increasing of MSE above an established baseline indicates that the system is foundering with consequent effects on the relative rate of penetration and other significant parameters.

From the data analysis of well 1, run 1, it is outlined that the average value for MSE is around 150 kpsi for the two run, considering a constant value for UCS of about 15 kpsi, the drilling efficiency is on the order of 10%. This result indicated that the small difference of the bits characteristics did not induce significant variations in the performances. In all the four analyzed cases it is possible to notice a massive presence of stick-slip and whirl due to the bit type and the horizontality of the hole.

Data related to the 4000 meters depth show a behavior due to a change in the lithology of the formation: the increase of the hardness induced the tool deviation and the increasing of the bending moment.

The WOB test performed in run 1 of Well 2 confirmed that when the drilling tool was operated in the linear region, e.g. in conditions of efficiency, MSE value remains constant value and close to its baseline.

The graph (at a depth from about 4730 to 4900 meters) shows also that the highest ROP value is not in correspondence with the highest WOB, suggesting that other parameters influence the system behavior which has been demonstrated by implementing the down hole well data to calculate ROP with the Borgounye & Young, (1974) model and by the relative ROP map showing the correlation between ROP, WOB and RPM.

In run 1 of well 2 it was possible to correlate the sudden increase of MSE and the severe decrease of ROP with the bit damage due to a too high WOB in correspondence of a formation with a higher rock strength. Hypothesis that was verified when in correspondence of another increase in rock strength (at a depth of about 5900 meters), the WOB was reduced instead of increased allowing the tool to fully penetrate the formation without damaging the bit.

Future researches will be related to the assessment of the measurement uncertainty, related either to the calculation of the model experimental coefficients or to the data acquired by the sensors. Sources of errors in the calculation of the significant parameters will be

identified and quantified. Moreover the research trend is to use the down hole data for feeding an intelligent systems for the management of well production.

REFERENCES

Armenta M., 2008, Identifying Inefficient Drilling Conditions Using Drilling-Specific Energy, Proc. of SPE Annual Technical Conference and Exhibition, Denver, Colorado.

Bourgoyne Jr., A.T., Young Jr., F.S., 1974, A Multiple Regression Approach to Optimal Drilling and Abnormal Pressure Detection, SPE Journal, Vol. 14(4): 371-384.

Caicedo U.P., Calhoun W.M., Ewy R. T., 2005, Unique ROP predictor using bit-specific coefficient of sliding friction and mechanical efficiency as a function of confined compressive strength impact drilling performance, SPE/IADC Drilling Conference. 2005, SPE: Amsterdam, The Netherlands.

Curry D., Christensen H., Fear M., Govzitch A., Aghazada L. 2005, Technical Limit Specific Energy - An Index to Facilitate Drilling Performance Evaluation, Proc. of SPE/IADC Drilling Conference, Amsterdam, Netherlands.

Dupriest, F.E. and Koederitz W.L., 2005, Maximizing Drill Rates with Real-Time Surveillance of Mechanical Specific Energy, in SPE/IADC Drilling Conference. SPE: Amsterdam, The Netherlands.

Guerrero C.A., Kull B.J., 2007, Deployment of an SeROP predictor tool for real time bit optimization, in SPE/IADC Drilling Conference. SPE: Amsterdam, The Netherlands.

Mohan K. and Adil F., 2009, Tracking Drilling Efficiency Using Hydro-Mechanical Specific Energy, in SPE/IADC Drilling Conference and Exhibition, SPE: Amsterdam, The Netherlands.

Morooka C.K., Guilherme I. R., Mendes J.R.P. 2001, Development of intelligent systems for well drilling and petroleum production, Journal of Petroleum Science and Engineering Vol. 32:191– 199.

Pessier R.C., Fear M.J., 1992, Quantifying common drilling problems with mechanical specific energy and bit-specific coefficient of sliding friction, in IADC/SPE conference, SPE: Washington D.C, USA.

Pessier R.C., S. Wallace and H. Oueslati 2012, Drilling Performance is a Function of Power at the Bit and Drilling Efficiency, in IADC/SPE Drilling Conference and Exhibition, SPE:San Diego, California, USA

Rashidi B., Hareland G., Fazaelizadeh M., Svigir M., 2010, Comparative Study Using Rock Energy And Drilling Strength Models, Proc. of 44th U.S. Rock Mechanics Symposium and 5th U.S.-Canada Rock Mechanics Symposium, Salt Lake City, Utah

Robinson L. H., Ramsey M. S., 2001, Are You Drilling Optimized or Spinning Your Wheels?, Proc. of AADE National Drilling Technical Conference, Houston, Texas.

Teale R., 1965, The concept of specific energy in rock drilling, International Journal of Rock Mechanics and Mining Sciences & Geomechanics, Volume 2 (1): 57–73

Waughaman R.J., Kenner J.V., Moore R.A., 2002, Real time specific energy monitoring reveals drilling inefficiency and enhances the understanding of when to pull worn PDC bits, in IADC/SPE conference, SPE: Dallas, Texas.

Shut in Pressure Test and Methods of Calculating Shut in Time in Fractured Low Permeable Oilfields Wells

Leng Tian[*1], Shunli He[2], Shijie Sun[3]

MOE Key Laboratory of Petroleum Engineering in ChinaUniversity of Petroleum, Beijing 102249
ChinaUniversity of Petroleum, Beijing 102249

[*1]ltianshen@sina.com; [2]zhanghl@cup.edu.cn; [3]isunshijie@gmail.com

Abstract

After oil wells were fractured, Pressure restore well test data of low permeable oilfields cannot test the straight line segment of radial flow easily. This paper analyzes the bottom hole flow characteristics in the earlier period of pressure restore test in fractured wells. Earlier flow in bottom hole is fracture single direction flow. It constructs a method for calculating the time of closing wells and measuring pressure in fractured oil wells using earlier well data. The method has practical application value, which can guide production.

Keywords

Low-permeable Oilfields; Production Wells; Transient Test; Shut-in Time And Measuring

Introduction

The content of well test includes the well production, pressure, temperature, sample of oil, gas or water etc. Based on fluid mechanics in porous medium, well test is used to confirm the production capability of the well, the physical property of the strata, the production performance, the boundary situation and the connection relationship between oil-water-gas strata through the usage of measurement instrument in production well or injection well. Well test is of crucial importance in petroleum reservoir engineering.

The two parts task of well test consists of data acquisition and data interpretation. The former is well site test and its major task is to collect enough reliable test data. The later one is well test interpretation and its task is to summarize more reliable information about the strata by the analysis of obtained data. These two parts are closely interconnected and interdependent. To get reliable well test interpretation is the goal of well test; and the prerequisite is to get accurate well test data. As a matter of fact, the quality and the quantity of well test results are determined by the quality and the quantity of data acquisition and the methods of data interpretation. At present, the interpretation methods technology is progressing parallel with the data acquisition advancement. And both of their progression is interconnected.

At present, the start time for shut-in pressure survey of oil well is based on the point where semilogstraightline occurred, which is also called mid-term section starting point or radial flow starting point. There are various judging criteria [1~5,10].Generally, the effective length in semilog radial flow straightline section for well test analysis should be less than two-thirds of log period. However, because wells start production after being fractured, the shut-in time for different wells are different, some buildup curves could not show boundary response to reflect true formation flow performance. Aiming at this problem, this paper proposed a new method to determine the effective shut-in time to reflect afterflow section, radial flow section and boundary response based on modern well testing theory and practical testing data in Changqing oilfield. This method could effectively reduce unnecessary testing time and increase effective testing time, which is useful for reference.

Background for Shutin Pressure Survey

Chang 2 reservoir in Sai 39 well area, ChangqingSuijing oilfield is low permeability reservoir. Well testing is an important method to evaluate formation dynamic performance. Transient test were applied in this area. According to the buildup test data, there were 23 sets of data in 19 wells showed constant pressure response, 31 sets of data in 23 wells showed no-mobile boundaries. No faults were found in this area and the no-mobile boundaries

were probably caused by lithological change or oil water interface around injection front.

Based on dynamic response, there were injection wells with no-mobile boundaries. The first time analysis result of injection well Lu 39-18 showed the existence of 2 no-mobile boundaries and the Lu 39-17 well on the west did not show effectual response. The second time analysis result still showed the existence of 2 no-mobile boundaries. Although the Lu 39-17 well on the west showed effectual response because fluid production, oil production and working fluid level all increased and water cut decreased. This effect should be caused by Lu 39-16 because the injection rate of Lu 39-18 decreased from 35m³/d to 20m³/d while the injection rate of Lu 39-16 stayed in 40m³/d. Lu 39-19 on the east did not show any effectual response.

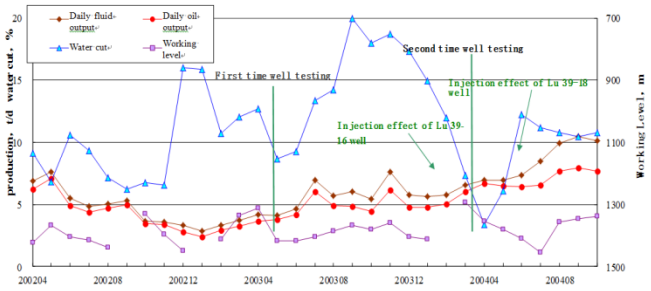

FIG.1 PRODUCING PERFORMANCE LU 39-17

But according to the recent dynamic response of Lu 39-17,there were effectual evidence that fluid production, oil production and working fluid level all increased and water cut decreased, the injection rate of Lu 39-16 stayed in 40m³/d and the injection rate of Lu 39-18 sharply increased from 20m³/d to 40m³/d, the cumulative injection were close to 2.0×10⁴m³,which might be caused by Lu 39-18.It shows that although perforation section did not coincide, there were still some hydrodynamic relations because there were not stable mud layer for insulation. When the injection rate was big enough or changed, the adjacent wells could be stimulated. So the no-mobile interface might be influenced by injection front. It is necessary to have more research on this topic.

Theoretical Model

Radial flow must be reached to obtain formation dynamic data for fractured wells, besides, the time for pressure to reach boundary should be considered.

For fractured wells, radial flow starting time correlates with fracture conductivity. According to empirical equation proposed in the paper: Oil and Gas Well Test Data Interpretation write by Ding Gui-ming[3,6], the equation for calculating radial flow is:

$$t_{Dbs} = 5\exp[-0.5(k_{fd} \cdot W_{fd})^{-0.6}] \quad (1)$$

$k_{fd} \cdot W_{fd}$ ——fracture conductivity, $10^{-3}\mu m^2 \cdot m$;

t_{Dbs} ——radial flow starting time, h.

According to the empirical equation proposed in the paper: Feasibility of analysis for shortening test time of low permeability reservoirs published in Petroleum Exploration and development[7], is the starting point where radial flow is reached：

$$t_{bs} = \frac{t_{Dbs}\phi \cdot C_t \cdot X_f^{\,2}}{3.6k}[(1-f_w)\mu_o + f_w \cdot \mu_w] \quad (2)$$

X_f ——fracture half length, m；

f_w ——water cut,%；

k ——permeability,$10^{-3}\mu m^2$；

C_t ——total compressibility,MPa^{-1}；

ϕ ——porosity,%；

μ_o, μ_w ——viscosity of oil and water, mPa • s.

For fractured wells, it is necessary to prolong buildup period to obtain qualified data. The buildup process was quite slow due to low pressure and low permeability. So the wellbore storage must be considered and the flowing time should be extended. According to the statistic of 54 sets of data in 42 wells, when the flowing time was three times the radial flow starting time, the error for interpreting formation parameter and pressure would be smaller, and it will be more accurate to judge boundary type.

Tripled radial flow starting time:

$$t_{bs}' = 3t_{bs} \quad (3)$$

Effective wellbore radius：

$$r_{we} = r_w^{-s} \quad (4)$$

In the equation: s ——skin factor；

r_w ——wellbore radius, m.

Applications

The average skin factor obtained from transient test for Lu 1-16,Lu 38-29,Lu 43-23 and Lu 42-15 wells in Chang 2 reservoir, Sai 39 well section, ChangqingSuijing oilfield is -4.3175.Combine skin factor with wellbore radius 0.062m, we can get effective wellbore radius r_{we}=4.65m.

Generally, facture half length in low permeability reservoir is 58.52m.Substitute it into effective wellbore radius equation r_{we}/x_f=0.07946, refer to the effective wellbore radius--finite conductivity vertical fracture relation schema[8~9].

$$k_{fd} \cdot W_{fd} = 0.29 \tag{5}$$

In the equation: k_{fd} ——permeability,10-3μm2;

W_{fd} ——width of fracture, m.

Substitute X_f =58.52m, ϕ =15.84%, C_t =17.57 1/MPa, μ_o =4.34mPa·s, μ_w =0.6575mPa·s, f_w =48.23% into equation (1),(2)and(3),we can obtain the flowing time that is three times the radial flow starting time(Table 1),we can see that the flowing time increases as the formation permeability decreases.

TABLE 1 THREE TIMES THE RADIAL FLOW STARTING TIME

K,10-3μm2	**3**	**4**	**6**	**10**	**15**	**20**
t_{bs}',d	50	37	25	15	9.9	7.4
K,10-3μm2	**25**	**30**	**40**	**50**	**60**	
t_{bs}',d	5.9	4.9	3.73	3	2.5	

Using Horner method, we can get radial flow starting time for Lu 39-17 and other 5 wells, the results are listed in table 2 and the Horner curve are Fig. 2.

TABLE 2 HORNER INTERPRETATION RESULT FOR TRANSIENT TEST

Well	**Lu 39-17**	**Lu 41-16**	**Lu 45-21**	**Lu 38-29**	**Tian 128**	**Lu 42-15**	**Conclusion**
Radial flow starting time, d	0.64	1.73	4.76	8.5	8.35	7.54	
Tripled radial flow starting time, d	1.9	5.2	14.3	25.5	25.0	22.6	
Boundary response starting point, d	3.9	6.9	8.9				
Test end time, d	24.0	22.6	15.7	15.0	13.0	14.8	25.0
Permeability,10-3μm2	45.44	27.42	9.93	6.63	6.13	6.76	6.0
Boundary type	Constant pressure	Constant pressure	Non mobile	Not occured	Not occured	Not occured	Boundary occured

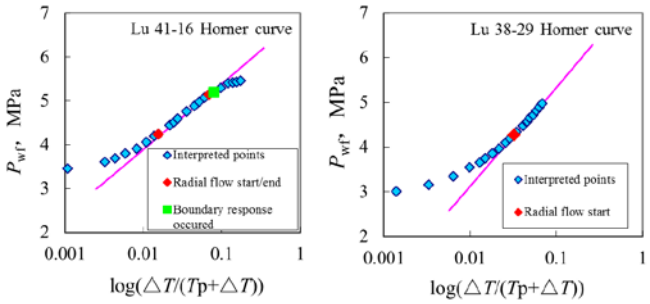

FIG. 2 LU41-16 AND LU 38-29 HORNER CURVE

From Table 2, it is easy to see that the test end time of Tian 128, Lu38-29 and Lu 42-25 are all shorter than tripled radial flow starting time, so Horner curve does not show boundary response, in comparison, test end time of Lu 39-17, Lu 41-16 and Lu 45-21 are all longer than tripled radial flow starting time, so we can determine boundary type from boundary response.

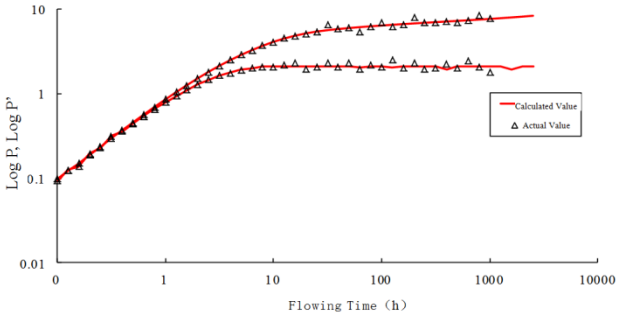

FIG. 3 LU38-29 UNREACHED BOUNDARY PRESSURE CURVE ANALOG

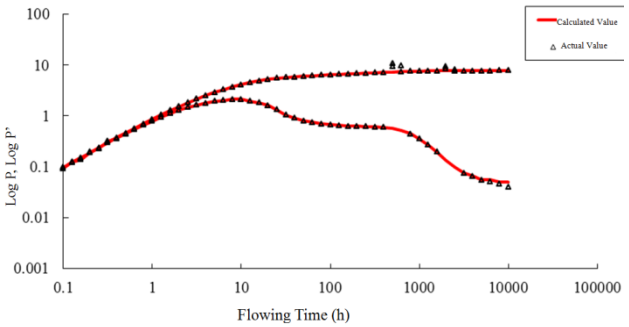

FIG. 4 LU 41-16 SINGLE BOUNDARY PRESSURE CURVE ANALOG

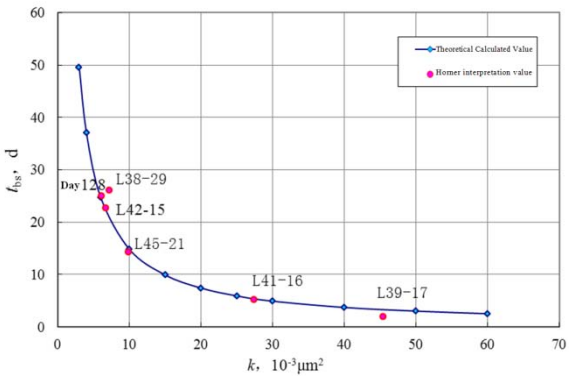

FIG. 5 TRIPLED RADIAL FLOW STARTING TIME—PERMEABILITY RELATION

According to boundary response, the test end time of Lu 38-29 is short that boundary response could not be observed (see Fig. 3). But Lu 41-16 reached radial flow period and we can observe boundary response (see Fig. 4).

It is easy to obtain tripled radial flow starting time—effective permeability relation scheme based on tripled radial flow starting time theoretical calculation equation (Table 1) and Horner interpretation result for transient test (Table 2).The results obtained from theoretical calculation equation and Horner interpretation are very close(see Fig.5).

So if we know effective permeability of certain formation, we can refer to the theoretical curve to obtain shut-in time for buildup test.

Conclusions

Conventional shut-in time could not obtain radial flow straightline section in low permeability wells so it's not suitable for calculating reliable formation pressure. This paper proposed an empirical method to calculate buildup test flowing time in low permeability reservoirs with smaller error and to determine the boundary type as well based on the data and the results provided above,. It could effectively save shut-in time to increase production.

ACKNOWLEDGMENT

The authors acknowledge a fund from the National Natural Science Foundation (NNSF) of China (No. 51204193) and supports from the MOE Key Laboratory of Petroleum Engineering.

REFERENCES

A. C. Gringarten, Analysis of an Extended Well Test to Assess Connectivity Between Adjacent Compartments in a North Sea reservoir, SPE Europec/EAGE Annual Conference, 13-16 June 2005.

Amin, A., Well Test Analysis of Infrequent Flow Behavior of Fractured Wells in Oil and Gas Reservoirs, SPE149887, 23 –25 January 2012.

A. O. Igbokoyi, D. Tiab, New Method of Well Test Analysis in Naturally Fractured Reservoirs Based on Elliptical Flow, Canadian International Petroleum Conference, Jun 17 - 19, 2008, Calgary, Alberta.

Ding Gui-ming, ectal. Oil and Gas Well Test Data Interpretation Model in China[M]. Bei Jing: Petroleum Industry Publication, 1994, 68-71.

FENG Feng ping. Amethod for calculating formation pressure in low permeable fractured well using earlier well test data [J]. Petroleum Geology & Oilfield Development in Daqing, 2005, 24(3): 63~65).

Gu Dai-hong, Liu Wei-ning, Deng Xian-Zhong. A study on falloff test in steam injection well [J]. Petroleum Exploration and development, 1997, 24(2): 66~68, 72.

Hao Yu-hong, Xu Min, Xu Xiao-rong. Accurately calculating dynamic reserves of low permeability gas reservoir[J]. Petroleum Exploration and development, 2002, 29(5): 66~68.

HuoJin, Jia Yong-lu, Jiang Wei-Jun. DST slug well test for low velocity non Darcy flowin dual-permeability reservoirs[J], Petroleum Exploration and development, 2005, 32(2): 98~100.

Lin Jia-en. The field experiment research of the reasonably measured presses the closed-in time in the development well [J]. Oil and Gas Well Test, 1996, 5(3): 24~29.

Lin Jing-ye, TongYing, LiuGai-qin. Optimum method for predicting the length of secondtime production test,[J]. PetroleumGeology&OilfieldDevelopmentinDaqing,1999, 18(3): 38~39.

LV Hong-bin,Yu Ying, Bie Ai-fang,ectal. Application of the zonal pressure testing data from east part of the north Block 3 in North Saertu, Daqing Oilfield[J]. Petroleum Exploration and development, 2004, 31(4): 120~122.

Mars Khasanov, VitalyKrasnov, TimurMusabirov, Special Issues of Well Test Design and Analysis for Fractured Wells in Waterflood, SPE Russian Oil and Gas Conference and Exhibition, 26-28 October 2010.

R. Aguilera, A Simplified Approach to Well Test Analysis of Naturally Fractured Reservoirs, SPE Canadian International Petroleum Conference, Jun 8 - 1, 2004.

Saud A. BinAkresh, SPE, and N.M. AnisurRahman, SPE, Challenges in Interpreting Well Testing Data from Fractured Water Injection Wells with a Dual Storage Phenomenon, SPE Middle East Oil and Gas Show and Conference, 25-28 September 2011.

Shi Zhong-qian, Yang Sheng-de. Feasibility of analysis for shortening test time of low permeability reservoirs[J], Petroleum Exploration and development, 2002, 29(3): 74~75.

S.-Y. Zheng and P. Corbett, Well Testing Best Practice, SPE Europec/EAGE Annual Conference, 13-16 June 2005.

Zhang Wei-qin, Chen He-ping. Postfracturing Gas-well-Test Analysis using Buildup Tyre Curves, 1994, 17(3): 50~55.